

TALLINN UNIVERSITY OF TECHNOLOGY
School of Information Technologies

Aleksei Veselkov 211960IVEM

Investigation of Energy Harvesting Methods During Testing Operations at a Telecom Company

Master's thesis

Supervisor: Yannick Le Moullec

PhD

Salvador Gonzalez
Perez

PhD

Tallinn 2023

TALLINNA TEHNIKAÜLIKOOL
Infotehnoloogia teaduskond

Aleksei Veselkov 211960IVEM

**Energiakorje meetodite uurimine
telekommunikatsiooniettevõtte testimise
keskkonnas**

Magistritöö

Juhendaja: Yannick Le Moullec

PhD

Salvador Gonzalez
Perez

PhD

Tallinn 2023

Author's declaration of originality

I hereby certify that I am the sole author of this thesis. All the used materials, references to the literature and the work of others have been referred to. This thesis has not been presented for examination anywhere else.

Author: Aleksei Veselkov

06.05.2023

Abstract

This MSc thesis is conducted in collaboration with a telecom company and aims at investigating suitable energy harvesting methods during radio equipment testing operations and assist the company in comprehending and gaining expertise on the concept of energy harvesting, with the goal of enabling them to utilize this knowledge to their advantage. To fulfil this goal, different aspects have been investigated and documented in this thesis.

First, it was required to get familiar with the testing procedures in the telecom company and determine the possible energy sources which could be used for energy harvesting.

Second, it was needed to analyse the various energy harvesting methods, their classifications, as well as to assess their suitability for the company's specific testing operations and internal processes. Along with that, the existing energy harvesting solutions available on the market were explored, and market trends were investigated.

During the third step, two available methods (radio frequency energy harvesting and thermal energy harvesting) were shortlisted as candidate methods to be implemented. Those methods were investigated more thoroughly, including reviewing best application practices and various technical implementation aspects. After reviewing of these two methods, it was concluded that the thermal energy harvesting method is the only one applicable for the given operational conditions and restrictions.

Finally, based on these findings, a thermal energy harvesting solution was proposed, developed, and verified. The resulting prototype consists of a thermal energy harvester and an energy converter. Design and verification included simulations and various real-life setups to determine the most viable solution for the operational conditions. As a result, recommendations are provided to the company in terms of possible implementations and ways for further research.

This thesis is written in English and is 73 pages long, including 6 chapters, 30 figures and 2 tables.

Annotatsioon

Energiakorje meetodite uurimine telekommunikatsiooniettevõtte testimise keskkonnas

Magistritöö on läbi viidud koostöös telekommunikatsiooniettevõttega, töö eesmärk oli leida sobilik energiakorje meetod raadio varustuse testimiseks ning nõustada ettevõtet energiakorje teemal, et ettevõtte saaks seda enda huvides rakendada. Selle eesmärgi täitmiseks on magistritöös uuritud ja dokumenteeritud erinevaid aspekte.

Kõigepealt tuli tutvuda telekommunikatsiooniettevõtte testimise protseduuriga ning teha kindlaks võimalikud energiaallikad, mida saaks energiakorjeks kasutada.

Teiseks tuli analüüsida erinevaid energiakorje meetodeid ja klassifikatsioone ning hinnata nende sobivust ettevõtte testimise protseduuri ja sisemiste protsesside jaoks. Uuriti ka turul olevaid energiakorje lahendusi ning turutrende.

Kolmanda sammuna vaagiti kahte kättesaadavat meetodit (energiakorje raadiosagedusel ja soojusenergiakorje), et leida milline neist on parim rakendamiseks telekommunikatsioonikompanii testimise läbiviimisel. Neid meetodeid uuriti süvitsi, sh analüüsiti parimaid kasutusjuhte ning mitmeid tehnilisi tahke. Peale kahe meetodi põhjalikku ülevaatusi tehti järeldus, et soojusenergiakorje on ainuke sobiv meetod olemasolevate tingimuste ja piirangute juures.

Lõpuks soovitati, arendati ning kontrolliti tulemustele põhinedes soojusenergiakorje lahendust. Tulemuseks on prototüüp, mis sisaldab soojusenergiakorjajat ja energiamuundurit. Kavandamine ja kontrollimine sisaldasid simulatsioone ja mitmeid elulisi olukordi, et teha kindlaks, milline tingimustele vastav lahendus on kõige paremini rakendatav. Selle tulemusena on ettevõtte jaoks välja töötatud soovitud rakenduse jaoks ning edaspidiseks uuringuks.

Lõputöö on kirjutatud inglise keeles ning sisaldab teksti 73 leheküljel, 6 peatükki, 30 joonist, 2 tabelit.

List of abbreviations and terms

3G	Third Generation
4G	Fourth Generation
5G	Fifth Generation
AUX	Auxiliary Port
CO ₂	Carbon Dioxide
DC	Direct Current
DTV	Digital Television
DUT	Device Under Test
EH	Energy Harvesting
E-WEHP	Embedded Wireless Energy-Harvesting Prototype
FOM	Figure Of Merit
GSM	Global System for Mobile communication
IC	Integrated Circuit
IoT	Internet of Things
LDO	Low Dropout
LTE	Long Term Evolution
MOSFET	Metallic-Oxide-Semiconductor Field Effect Transistor
MPTT	Maximum Power Point Control
NR	New Radio
PC	Personal Computer
PCB	Printed Circuit Board
PWL	Piecewise Linear
RF	Radio Frequency
RX	Receiving
SPICE	Simulation Program with Integrated Circuit Emphasis
TEC	Thermoelectric Cooling
TEG	Thermoelectric Generator
TEH	Thermoelectric Harvester

TV	Television
TX	Transmission
UMTS	Universal Mobile Telecommunications System
WSN	Wireless Sensor Network

Table of contents

1	Introduction	15
1.1	Problem statement	16
1.2	Thesis tasks.....	17
1.3	Thesis organisation	18
2	Background on energy harvesting methods.....	19
2.1	Classification of energy harvesting methods.....	19
2.2	Market trends	22
2.3	Existing integrated circuits for thermal and RF energy harvesting solutions.....	24
2.4	Energy harvesting issues and challenges.....	25
3	Analysis of sources of wasted energy at the telecom company	28
3.1	Available sources of wasted energy	28
3.2	Selection of a suitable energy harvesting method	32
3.2.1	Thermal energy harvesting	32
3.2.2	RF energy harvesting.....	33
4	Developed thermal energy generator hardware solution and simulation results.....	37
4.1	Design.....	37
4.2	Implementation.....	39
4.2.1	TEG	39
4.2.2	TEG output parameters and effectiveness estimation	40
4.2.3	TEG output conversion.....	43
4.2.4	SPICE simulation results.....	46
5	Real-life experiments.....	51
5.1	Testing of the TEG	51
5.2	Experiments on TEG effectiveness	58
5.3	Experiments with the TEG output conversion	59
5.4	Discussion of the results.....	63
6	Conclusion.....	65
6.1	Summary and main findings.....	65

6.2 Recommendations for further work.....	66
References	67
Appendix 1 – Non-exclusive licence for reproduction and publication of a graduation thesis	73

List of figures

Figure 1: Classification of energy sources for EH [9]. The energy sources categories are defined as thermal, light, electromagnetic (EM), RF, chemical, and mechanical. Each category is itself divided into subcategories, which represent matter or phenomenon as the energy source. 20

Figure 2: Global energy harvesting market by technology [24]. The thermoelectric EH technology proportion is around 46%, compared to electrodynamics, piezoelectric and photovoltaic proportion all together, although RF EH falls into other parts and takes less than 2%. 22

Figure 3: Example of a thermal electric generator commercial solution [25]. It consists of a heat absorber, a cooling system and a power regulating circuit and integrated as an all-in-one device..... 23

Figure 4: Graphical representation of a possible testbed for radio unit testing. The signal generators are connected to the DUT inputs. Measurement equipment (oscilloscope, power meter, network analyser) is connected to the DUT output. The test operator controls test scripts set up, execution process and test results on the PC..... 29

Figure 5: Graphical representation of a test setup with an anechoic chamber. The internal surfaces of the chamber are covered with RF absorbent material. The DUT is placed inside of the chamber and radiates radio signals during the test. Measurement antenna connected to measurement equipment, which are placed outside of the chamber. 31

Figure 6: TEG diagram for self-powered application [37]..... 33

Figure 7: Block diagram of RF-EH Solution [44]. 35

Figure 8: Schematic diagram of Peltier thermoelectric couple, consisting of n-type and p-type thermoelectric materials [49] a) refrigeration mode when the current I applied to the Peltier element input and b) power-generation mode, when the current I generated on Peltier element inputs if temperature difference applied to the Peltier element surfaces. 38

Figure 9: Proposed TEG assembly illustration (side view, corresponding to 1 row of 5 Peltier elements) 39

Figure 10: Photograph of the initial developed prototype TEG assembly with 15 Peltier elements for the proposed TEG. Notice that the elements are not connected, which allows testing different configurations of series and parallel connections.	40
Figure 11: Estimated output voltage V of the single TEC depending on temperature difference ΔT ($^{\circ}\text{C}$)	41
Figure 12: Bismuth telluride based TEG's effectiveness estimation η_{max} (%), depending on temperature difference between the hot and cold sides ΔT ($^{\circ}\text{C}$)	43
Figure 13: LTC3108 block diagram for the typical application [56].	45
Figure 14: The assembled circuit for LTC3108 (marked LTC3108) and external components (transformer and capacitors).....	45
Figure 15: Equivalent schematics of the assembled DC converter circuit for LTC3108 for simulation purposes.	46
Figure 16: SPICE simulation results for LTC3108 DC converter with input increase from 0.01V to 1V during 1 s. The input voltage V_{in} is shown with the purple line on the chart, the output voltage V_{out} with the blue line, and V_{LDO} with the brown line and V_{aux} with the green line.	47
Figure 17: SPICE simulation result for LTC3108 DC converter with input decrease from 0.889V to 0.02V during 1 s and keep the input at 0.02V during next 3 s. V_{in} is shown with a purple line on the chart, V_{out} with the blue line, and V_{LDO} with the brown line and V_{aux} with the green line.....	48
Figure 18: SPICE simulation result for LTC3108 DC converter with input decrease from 0.889V to 0.02V during 1 s and drops further during the next 3 s to 0.01V. V_{in} is shown with the purple line on the chart, V_{out} with the blue line, and V_{LDO} with the brown line and V_{aux} with the green line.....	49
Figure 19: Radio equipment DUT temperature T ($^{\circ}\text{C}$) measurements during load test during test execution time t (min).....	51
Figure 20: Temperature difference ΔT ($^{\circ}\text{C}$) during test execution time t (min).	52
Figure 21: Schematic representation of proposed TEG connection diagram (all Peltier elements connected in series) for achieving the maximum voltage output.....	53
Figure 22: Measurement results with all Peltier elements connected in series for achieving the maximum voltage output (schematic of Figure 21):measured voltage output Voltage (V) of the TEG (red line), temperature difference of the DUT surface and ambient temperature ΔT ($^{\circ}\text{C}$) (blue line), and temperature difference between the hot and cold sides of the TEG ΔT ($^{\circ}\text{C}$) (brown line).	54

Figure 23: Schematic representation of proposed TEG connection diagram for the purpose of increasing the current output I_{TEG_max} ; The Peltier elements are organized as 3 rows wherein the 5 elements connected in series. The rows are connected in parallel.. 55

Figure 24: Measurement results with the Peltier elements organized as 3 rows wherein the 5 elements connected in series and the rows are connected in parallel, for the purpose of increasing the current output I_{TEG_max} (schematic of Figure 23):.measured voltage output Voltage (V) of the TEG (red line), temperature difference of the DUT surface and ambient temperature ΔT ($^{\circ}C$) (blue line) and temperature difference between hot and cold side of the TEG ΔT ($^{\circ}C$) (brown line)..... 56

Figure 25: Measurement results on one single Peltier element on the TEG (one element from the schematic of Figure 23): measured voltage output Voltage (V), (red line), temperature difference of the DUT surface and ambient temperature ΔT ($^{\circ}C$) (blue line) and temperature difference between hot and cold side of the TEG ΔT ($^{\circ}C$) (brown line) 57

Figure 26: TEG effectiveness calculation based on the experimental results; η_{max} % is the effectiveness of the TEG and ΔT ($^{\circ}C$) is the temperature difference obtained on the TEG cold and hot surfaces. 58

Figure 27: DC converter output graph for TEG elements connected in series. The TEG output is represented with the red line and labelled as V_{teg_out} , DC converter V_{out} is represented with the blue line (labelled as V_{out}) and V_{LDO} output of DC converter is represented with the brown line (labelled V_{ldo}). 60

Figure 28: DC converter output graph for TEG elements, connected in series and parallel. The TEG output is represented with the red line and labelled as V_{teg_out} , the DC converter V_{out} is represented with the blue line (labelled as V_{out}) and the V_{LDO} output of DC converter is represented with the brown line (labelled V_{ldo}). 61

Figure 29: DC converter output graph for a single Peltier element of TEG. TEG Peltier element output is represented with red line and labelled as V_{teg_s} , DC converter V_{out} represented as blue line (labelled as V_{out}) and V_{LDO} output of DC converter represented with brown line (labelled V_{ldo}). 62

Figure 30: Proposed energy conversion schematic with 3 DC converters, connected to 5 Peltier elements each. The Peltier elements are connected in series. $V_{TEG_out 1}$ is the output from the first 5 Peltier elements in the top row, $V_{TEG_out 2}$ is the output from the second 5 Peltier elements in the middle row, and $V_{TEG_out 3}$ is the output from the third 5 Peltier

elements in the bottom row. V_{out} , V_{out2} and V_{out3} are the outputs from the first, second, and third DC converter, respectively..... 64

List of tables

Table 1: Comparison of integrated circuits for energy harvesting	25
Table 2: Examples of typical energy sources power levels.....	26

1 Introduction

The world is facing the urgent challenge to reduce greenhouse gas emissions and combat climate change [1]. Many countries, companies, and organizations have made pledges to achieve carbon neutrality by 2050 [2]. Carbon neutrality (also referred to as “Net Zero”) refers to achieving a balance between the amount of greenhouse gas emissions produced and the amount removed from the atmosphere. This can be achieved through various measures such as reducing emissions, implementing renewable energy sources, and using carbon capture and storage technologies. The pledges for carbon neutrality by 2050 represent a major shift towards a sustainable and low-carbon economy. Achieving carbon neutrality by 2050 will require significant investments in research and development, infrastructure, and technology. It will also require a coordinated effort among governments, businesses, and individuals to reduce emissions and adopt sustainable practices [3].

The benefits of achieving carbon neutrality by 2050 are numerous, including reducing the risks associated with climate change, promoting energy security, and creating new economic opportunities. However, there are also challenges associated with the transition to a low-carbon economy, including the need for considerable policy changes, the high costs of transitioning, and the potential social and economic impacts. An additional challenge is the deployment and integration of sustainable technologies, which could require ongoing investment into research and innovation [4].

To comply with climate change regulations and reduce carbon footprint, companies may need to adapt their strategies, policies, and practices by promoting sustainable and renewable energy sources, improving energy efficiency to contribute to the global effort. Developing new strategies can also help companies reduce their energy consumption, which can result in lower operating costs. As an example, the implementation of energy harvesting (EH) solutions is a potential approach to employ technologies focused on the reuse of wasted energy, which could be a key component of such strategies.

In this context, energy harvesting (EH) methods are increasingly becoming attractive for researchers and practitioners. EH methods seek to exploit different ambient energy sources, such as solar, thermal, vibration and mechanical.

This MSc thesis is conducted in collaboration with a telecom company. In this type of company, the investigation of energy harvesting methods has been identified as a desirable opportunity to find a feasible solution to reuse energy during testing processes (of e.g., radio units) by harvesting and repurposing some of the emitted energy that would otherwise be wasted. However, in comparison to existing ambient energy harvesting methods with low-power levels (e.g., μW), the methods of energy harvesting during radio unit testing need to be redesigned since direct energy harvesting will be carried out and the power levels of the emitted energy could be significantly higher (e.g., W vs. μW).

In this work, the focus is on thermal and RF energy harvesting methods; indeed, those two energy sources have been identified as available during in-the-field testing operations at the telecom company. The description of those methods is given in application to the telecom company internal process; they are briefly introduced in Chapter 2 and discussed in greater details later in Chapter 3.

1.1 Problem statement

EH is a set of promising methods and technologies, but at the same time it is challenging in various aspects including design and implementation. Even though a wide range of approaches exists, they are only suitable for ambient energy harvesting [5] for e.g., the Internet of Things (IoT) or powering low-power integrated circuits and small devices. In other words, existing energy harvesting methods are aimed at processing and managing energy on very low power levels. Along with that, the effectiveness and feasibility of methods and approaches remain an issue since certain limits exist. As an example, ambient RF energy has a low energy density of 0.2 nW/cm^2 to $1 \text{ }\mu\text{W/cm}^2$, and an efficiency of about 38-39%. Thermal EH power density is estimated from $30 \text{ }\mu\text{W/cm}^2$ to 10 mW/cm^2 (depending on the temperature levels) with an efficiency of 5-15% [5].

There are demanding requirements to those solutions because they operate within very low power conditions. However, the existing methods could be examined and reused to explore those limits and additional factors, which influences the effectiveness. For a

telecom company it is an area of the interest, so there is a challenge to investigate EH methods to increase their knowledge on the topic and analyse advantages and disadvantages.

Given the above, the problem statement of this MSc thesis is expressed as a series of questions:

- What energy harvesting methods exist and what are their main properties?
- What are the main characteristics of the telecom company testing environment and operational conditions, including possible different EH and alternative opportunities in terms of energy sources?
- What are the main factors which influence the feasibility of energy harvesting approach considering the manufacturer testing methodology?
- What are the viable solutions for developing a proof-of-concept of energy harvesting? Options to be investigated include off-the-shelf components, custom designs, or a combination thereof.
- Based on the findings from the above, what suggestions and recommendations in the form of design concepts, simulation results, and implementation results can be made?

1.2 Thesis tasks

The goal of this MSc thesis is to study EH methods, exploring the potential for energy harvesting possibilities at a telecom company. Another goal is to design and implement functional EH solutions, conduct practical experiments and verify factors that may have influence on effectiveness, output parameters and feasibility of use. To achieve these goals, the following tasks have been conducted:

1. Conduct a literature review on energy harvesting technologies and their application in various industries.
2. Evaluate existing solutions, viable for energy harvesting purposes at a telecom company during testing operations.

3. Analyse and evaluate fit-for-purpose energy harvesting technologies in terms of efficiency, reliability, cost-effectiveness, and scalability.
4. Design and implement an energy harvesting system as a prototype.
5. Conduct experiments and performance evaluation of the energy harvesting system, including testing for efficiency, energy output, and reliability.
6. Evaluate the sustainability, reliability, and feasibility of energy harvesting system.
7. Identify and analyse strengths and weaknesses of the designed systems, propose improvements, and give recommendations for further development, research, and usage.

1.3 Thesis organisation

The rest of this MSc thesis is organized as follows: Chapter 2 presents the overview of the EH methods, their classification, and outlines existing solutions and challenges. Then, Chapter 3 delves into the energy sources used at the telecom company during testing processes that would be available for EH, and the selection of corresponding EH methods for conducting experiments. Following the selection of the thermal electric EH method, Chapter 4 introduces the thermal electric EH system developed as part of this thesis, i.e., its design and its main elements, including the hardware solution and corresponding simulation results. Chapter 5 presents and analyses the in-the-field experimental results of the developed thermal electric EH system, including its performance and effectiveness analysis. Finally, Chapter 6 concludes the thesis with a summary, main findings/suggestions, and briefly outlines possible future work.

2 Background on energy harvesting methods

The aim of this chapter is to provide a review of available EH methods, including their underlying principles, working mechanism, and possible applications. The chapter describes the different types of energy sources that can be harvested and gives an overview of EH methods classification, market trends, and existing solutions. Moreover, the chapter introduces the main EH challenges and drawbacks when designing efficient and sustainable EH systems.

2.1 Classification of energy harvesting methods

Nowadays the subject of EH is very much focused on powering IoT and WSN devices including the introduction of battery-less solutions for low power devices [6]. Those devices (e.g., health care devices, placed in human body, sensors in the sea and oceans, weather sensors) could be placed in the remote areas, which brings a challenge to take care of battery-based power supply. At the same time, despite the technological progress achieved in terms of energy efficiency in low-power integrated circuits, embedded solutions, and sensors, the characteristics of chemical batteries have not developed as rapidly and still need to be improved to meet requirements such as size, durability, and safety. Therefore, contemporary research is focused on developing new EH approaches to meet all requirements of self-powered systems.

However, EH has also found applications in various areas related to repurposing wasted energy in industrial and manufacturing processes, showing promising results and feasibility [7], [8]. This makes energy harvesting approaches and methods applicable for increasing energy efficiency as a part of zero-energy manufacturing business strategies, together with decreasing energy consumption and CO₂ emissions. Building these strategies requires a deep analysis of wasted energy sources, applicable harvesting methods, feasibility of these methods, storage of otherwise wasted energy, and ways of reusing this harvested and stored energy.

EH can be classified in different ways: by energy source, by harvesting method/mechanism, and by purpose. Each approach, in turn, can be divided into smaller categories and sub-categories, depending on methodology and scalability.

However, in the case where the goal of EH lies in energy repurposing, it is advisable to classify these methods by available energy sources, then analyse the amount of wasted energy that could be repurposed and study the feasibility of the approaches.

Energy sources available for EH can be divided into the following groups:

- Ambient energy: sunlight, ambient heat, wind, environmental mechanical energy (such as hydro or ocean waves energy harvesting).
- External energy: explicit energy, such as vibrations, lightning, wasted heat, wasted electromagnetic radiation, mechanical, etc.

External energy sources could be considered as the intrinsic sources available during manufacturing operations in the industry. Compared to ambient energy sources, they are more stable, measurable, and predictable, as well as non-dependent on environmental conditions, such as weather and insulation levels.

In what follows, let us consider the classification by energy sources for which a classification diagram is shown in Figure 1 [9].

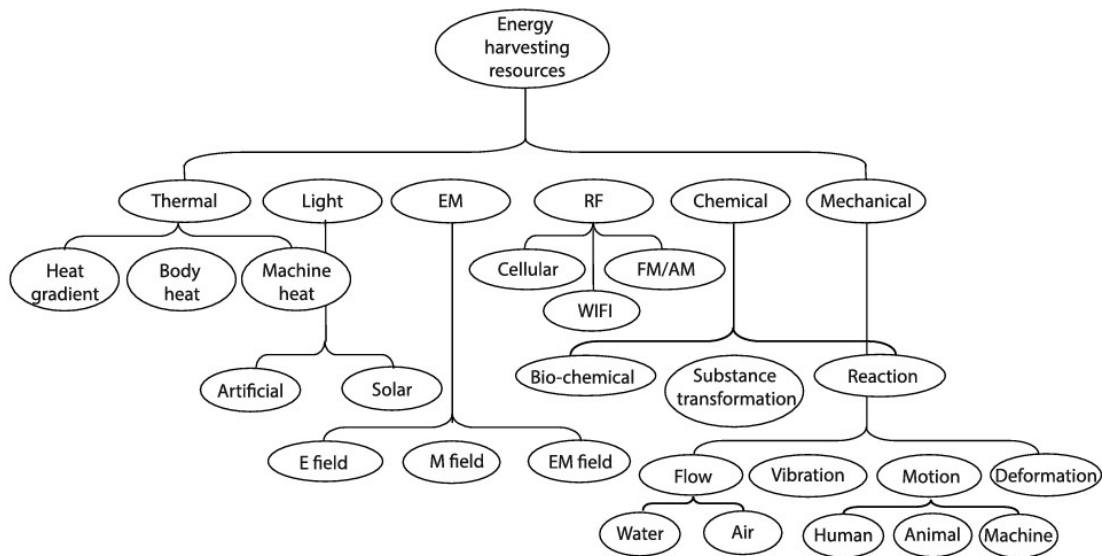


Figure 1: Classification of energy sources for EH [9]. The energy sources categories are defined as thermal, light, electromagnetic (EM), RF, chemical, and mechanical. Each category is itself divided into subcategories, which represent matter or phenomenon as the energy source.

EH approach from different sources may vary, depending on available technology, amount of power produced by energy source and the purpose. A typical energy harvesting

device consists of 1) an energy capturing element, providing the possibility to convert energy from its source form into electrical energy; 2) a conversion unit element, which includes the circuitry providing regulation and protection, and 3) a storage element, for storing electrical energy in some form, typically but not exclusively for later use.

What follows briefly introduces the three main categories of initial interest to the telecom company: thermal, RF, and mechanical.

Thermal energy harvesting (TEH)'s principle depends on a thermoelectric generator (TEG) operation. It converts thermal energy directly into electrical energy according to the Seebeck effect [10], [11]. An example of a heat source could be an industrial machine that operates at high temperature and dissipates the heat to the ambient air; for instance, engines, electric transformers, or heat exchangers, although TEGs are widely used for harvesting energy from low temperature sources, such as human body [12]. The amount of harvested energy from these sources varies depending on the approach, type of the element, and technology used [13].

Radio frequency energy harvesting (RF-EH) is an approach used to capture the electromagnetic energy emitted from RF sources (TV and radio signals, cell towers, wireless transmitters) and convert it to direct current (DC) for further repurposing, typically in low-power demanding devices. One of the aims of RF-EH is to contribute to autonomous embedded devices and systems that normally uses batteries or are directly connected to the power source. Harvested RF energy is commonly used for applications for which it is difficult or impossible to change the batteries. RF-EH has been rather extensively researched, as reflected in several survey papers related to this topic, see for example [14], [15], [16], [17].

Mechanical energy harvesting can be achieved using various techniques, such as piezoelectricity, electromagnetic induction, and electrostatics to convert mechanical energy from vibration, motion and pressure into electrical energy [18]. Piezoelectric materials transform mechanical force into electrical power [19], while electromagnetic generators use the motion of magnets and coils to generate electricity [20]. Electrostatic generators use the principle of triboelectricity to generate an electric charge when two different materials come into contact and then separate [21]. These techniques could be

used to generate electrical energy from such sources, as vibrations of the industrial equipment, vehicles, bridges or buildings, as well as human kinetic motion.

As this thesis is focused on the EH methods investigation for a testing process in a telecom company, and not all the EH methods are applicable for this process. The two energy sources that have been identified during in-the-field testing operations, i.e. thermal and RF EH methods, are studied more thoroughly; the criterion of the methods selection and analysis are provided later in Chapter 3.

2.2 Market trends

An EH market trends analysis and forecast for 2018 – 2024 [22] show that this market has been growing over the last years and will continue its growth of 7.5% in the nearest years and is expected to reach \$1,057 Billion by 2030 [23]. The reason is the increased interest in green energy and renewable energy sources. As mentioned in the market research, along with the most common energy sources that are solar and wind energy, other technologies are widely used as well. Figure 2 gives an overview on the technologies used for energy harvesting in small-scale energy harvesters for IoT, wherein thermoelectric EH alone makes 46%.

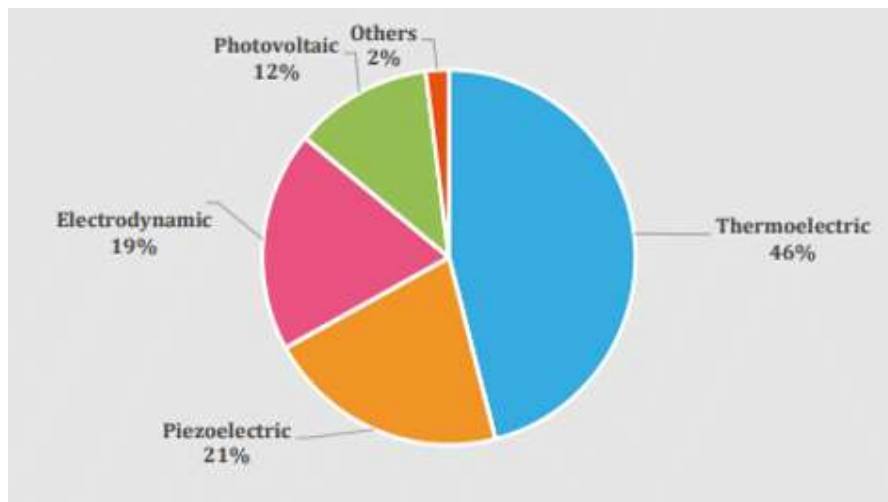


Figure 2: Global energy harvesting market by technology [24]. The thermoelectric EH technology proportion is around 46%, compared to piezoelectric, electrodynamics, and photovoltaic combined together (52%); RF EH falls into the “others” category and makes less than 2%.

The primary methods for growth pursued by companies in the EH system market is to expand their business and acquiring other businesses. Growing demand for energy harvesting is also observed in Industry 4.0 strategies implementation.

Many companies finds their niche in the development and distribution of complete set of energy harvesters, mostly based on thermoelectric harvesting technologies. As an example, commercial solutions of TEGs are used as a set-top for wooden and gas stoves to generate a certain amount of energy which could be used in emergency situations, for example to recharge batteries, mobile phones, and use this energy for emergency radio, lighting, or mobile communication. An example of such a solution is shown in Figure 3.

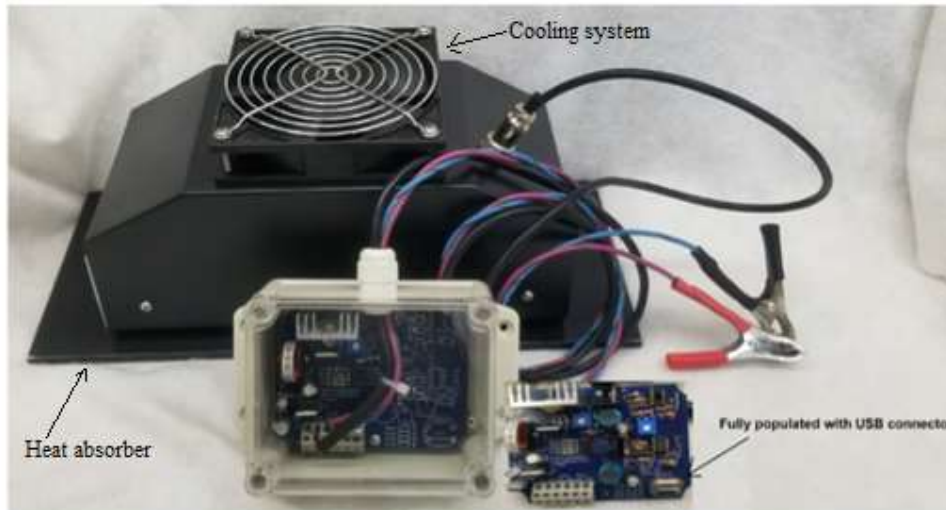


Figure 3: Example of a thermal electric generator commercial solution [25]. It consists of a heat absorber, a cooling system and a power regulating circuit integrated as an all-in-one device.

As for alternative EH technologies (e.g. RF, piezoelectric, electrodynamic and others), there are no common approaches and standards [26], so they find their applications in ad-hoc ways.

A clear trend in the market is the increasing use of EH in building automation systems. Building automation systems require a significant amount of power to operate, and energy harvesting technologies are being used to power sensors, switches, and other components, reducing the overall energy consumption of the building [27].

The automotive industry is also a growing market for EH technologies, with applications in tire pressure monitoring systems, engine management systems, and other areas [28].

Thus, the energy harvesting market will continue growing, primarily due to the increasing demand for energy-efficient solutions and sustainable power sources. The growing trend of miniaturization of electronic devices and sensors has also led to an increase in the demand for EH technologies that can provide a sustainable power source for these devices without the need for frequent maintenance or replacement of batteries.

2.3 Existing integrated circuits for thermal and RF energy harvesting solutions

Considering the existing integrated circuits, aimed to solve technical issues such as the instability of the energy sources, there are several solutions available on the market. An overview of the most commonly used integrated circuits for thermal and RF EH is given in Table 1.

Table 1: Comparison of integrated circuits for energy harvesting

Type	Name	Manufacturer	Description	Output Voltage	Quiescent Current (I _q)	Sensitivity
Thermal	LTC3108	Linear Technology	Highly integrated DC/DC converter	4.6 V	80 nA	20 mV
	bq25505	Texas Instruments	Low power harvester power management IC	5.0 V	325 nA	100 mV
	SPV1050	STMicroelectronics	Ultra-low power and high-efficiency power manager	3.6 V	Not specified	180 mV
RF-EH	MAX11710	MAXIM	Complete system for charging and protecting micropower-storage cells	6.0 V	625 nA	0.75 V
	PCC110	Powercast	RF-to-DC converter and the boost converter for 100MHz-6GHz	-	75% of peak efficiency	-17 dBm
	AEM30940	e-peas	High frequency 868MHz or 915Mhz RF input harvester with LDO	4.5 V	400 nA	-19 dBm

2.4 Energy harvesting issues and challenges

While EH becomes increasingly popular, there are still major challenges to deal with. The power levels are often low (due to low power densities) and unstable [5]. Examples of power densities are shown in Table 2.

Table 2: Examples of typical energy sources' power densities

Energy source	Power density
Vibration	Human: $4 \mu W/cm^2$ Industrial: $100 \mu W/cm^2$
Thermal	Human: $30 \mu W/cm^2$ Industrial: $1-10 mW/cm^2$
RF	GSM: $0.1 \mu W/cm^2$ WI-FI: $1 mW/cm^2$

In case of RF-EH, the power of the emitted radio signal will attenuate with distance, especially in higher frequency ranges.

Only devices operating on very low power levels can be coupled (and be directly operated) with such energy harvesters. It is possible that the power supply of the device stops, so sudden shutdown of the power supply should be considered. Power management becomes one of the challenges that EH faces [29].

Moreover, the efficiency of energy harvesting devices is typically lower than conventional energy sources. For example, RF-EH devices could have a maximum efficiency of 38-39 % [5]; however, TEGs have maximum efficiency of 15 % or even lower [30].

Energy storage and use of this energy is a challenge as well, since most of the energy harvesting solutions are intermittent and thus not reliable. Most of the EH approaches are considered as a supplement to the battery supply and cannot be used independently, unless special methods are implemented, such as intermittent computing mechanisms relying on non-volatile memories in microprocessor-based systems [29].

The EH devices and solutions are costly due to their complexity and large amount of components required. Developing highly efficient and productive solutions becomes another challenge, combining best practices and eliminating restrictions and finding workarounds for limitations. For IoT devices or WSN solutions it is sometimes needed to use a combination of EH devices to reach power autonomy, which additionally increases costs [26].

The size of the EH devices can be large as compared to standard batteries, especially when there is a need to create a versatile harvester to retrieve energy from multiple sources. To harvest energy in a comparable amount to that of a battery capacity, it is required to make an assembly comprising multiple elements. For instance, the typical dimensions of a thermoelectric element is 40 *mm* wide and 40 *mm* long, and it is required to assemble several of them for harvesting a useful amount of energy. The same applies to solar panels. Every EH solution requires power management electronic circuit designed specifically.

Finally, there is no international standards for energy harvesters, as well as precise techniques and best practices for common solutions. Creating a standard on measurements, energy storage, and design methodologies will decrease costs and facilitate the innovations and development in this area [26].

At this point in this thesis, it should be noted that no off-the-shelf solution has been identified as 'obviously' suitable by the telecom company, which justifies the need to continue exploring possible options and solutions. That said, the rest of this thesis does not provide an exhaustive analysis of all aspects of EH solutions. Instead, this document introduces viable methods for the telecom company, based on the available energy sources during their operations, and analysing by means of experiments the effectiveness and feasibility of the typical approaches. Moreover, this work does not give a comprehensive review of the energy storage mechanisms, as this is not in the scope of this thesis goal.

To sum-up, this chapter outlined available EH methods, their classification, working mechanisms, as well as trends and existing solutions. In the next chapter, available energy sources at the telecom company are analysed, appropriate EH methods reviewed and described more thoroughly.

3 Analysis of sources of wasted energy at the telecom company

This chapter introduces the identified sources of wasted energy at the telecom company during testing process and provide the overview of suitable EH methods for these sources.

Determining and analysing wasted energy sources is a first step in building a company's strategy for energy repurposing. This task becomes more challenging if manufacturing processes includes precise measurements during the production cycle, where any intrusion to the process may affect the results. For instance, introducing an electromagnetic wave power energy harvesting device into the transmission line could affect the resulting signal parameters at the output of the transmission line. Therefore, special attention must be given to the selection of waster energy sources and possible corresponding EH method.

3.1 Available sources of wasted energy

To identify the specific sources of wasted energy in testing process, it is essential to analyze the testing methodology and equipment. Radio unit testing process involves a series of steps to ensure that the radio unit functions properly and meets the required specifications. Different types of tests are typically conducted:

- TX test to verify transmission parameters of a radio unit.
- RX test to verify receiving parameters of a radio unit.
- Burn-in and load test to determine a radio unit behavior under most rigorous, extreme, or extended working conditions, including normal and peak load conditions.

A mobile radio unit can operate in different modes and frequency bands, so it is necessary to design and execute precise test scenarios for different conditions, as well as to setup a specific testbed. Tests scripts are automated and do not require manual steps execution during test run. The radio unit's RF performance is tested to ensure that it meets the required specifications for transmit power, receive sensitivity, and interference rejection. This involves testing the radio unit in a controlled RF environment using specialized test equipment.

Let's consider a possible testbed used for radio unit testing. The setup may vary, depending on the test type and objectives; however, in general the testbed consists of the following parts:

- Different types of signal generators, which are used for generating a wide range of RF signals with varying frequencies, modulation, and power levels.
- Oscilloscope, used for visualizing and analyzing the radio unit's waveforms.
- Power meter, used for measuring the radio unit's transmit power and receive sensitivity.
- Network analyzer, used for measuring the radio unit's insertion loss, return loss, and isolation.
- Operator PC, used to setup, control, execute, analyze, and report test scenarios.

A typical setup requires connecting the signal generators to device under test (DUT) inputs and measurement equipment to the DUT outputs. The test operator uses the PC, connected to the equipment, to manipulate the test data, test setup, execution process, and analysis and reporting of the results. A graphical representation of such a testbed for radio unit testing is shown in Figure 4.

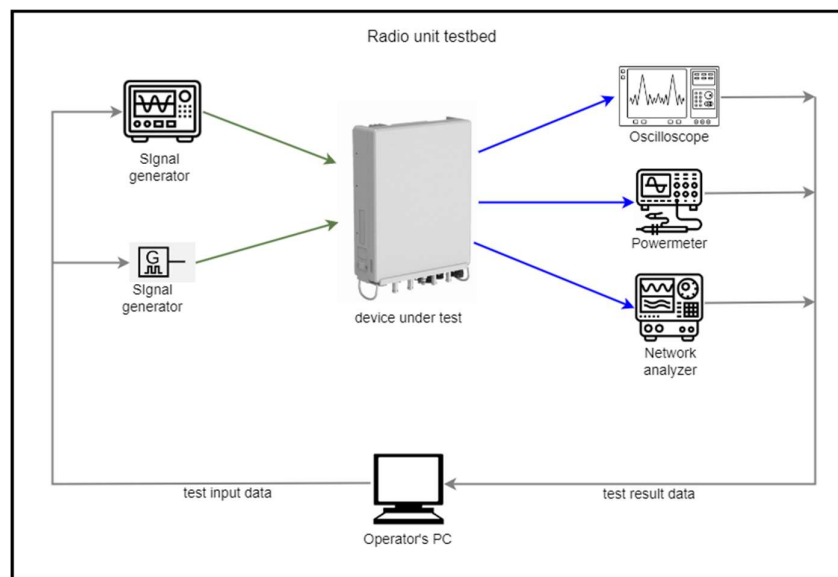


Figure 4: Graphical representation of a possible testbed for radio unit testing. The signal generators are connected to the DUT inputs. Measurement equipment (oscilloscope, power meter, network analyser) is

connected to the DUT output. The test operator controls test scripts set up, execution process and test results on the PC.

The equipment listed above is placed in stand and racks and is interconnected together. The stand is used to place and reliably fix the DUT and connect it properly to the measurement units in the testbed itself in a convenient way. It also allows working with different types of DUTs with different sizes and parameters.

The described testbed is used for a wide range of different test types, including load and performance tests. During the load and performance tests, the DUT heats up while the tests are executed. As per specification, the DUT's temperature may reach up to 80 °C, depending on the test scenario.

Another type of testbed used in radio unit testing process is a specific setup within an anechoic chamber. An anechoic chamber is a room specially designed for RF and used for testing and measuring RF signal parameters. The walls, ceiling, and floor of an RF anechoic chamber are lined with specialized materials such as ferrite tiles, pyramidal foam absorbers, or metallic honeycomb structures. These materials are designed to absorb electromagnetic waves and radiofrequency signals, preventing any reflection or interference that could affect the accuracy of the measurements. The RF anechoic chamber is equipped with measurement equipment, such as an antenna or a probe, and a DUT is placed on a test bench. The measurement equipment is used to measure the performance and characteristics of the DUT. A graphical representation of an anechoic chamber testbed is shown in Figure 5.

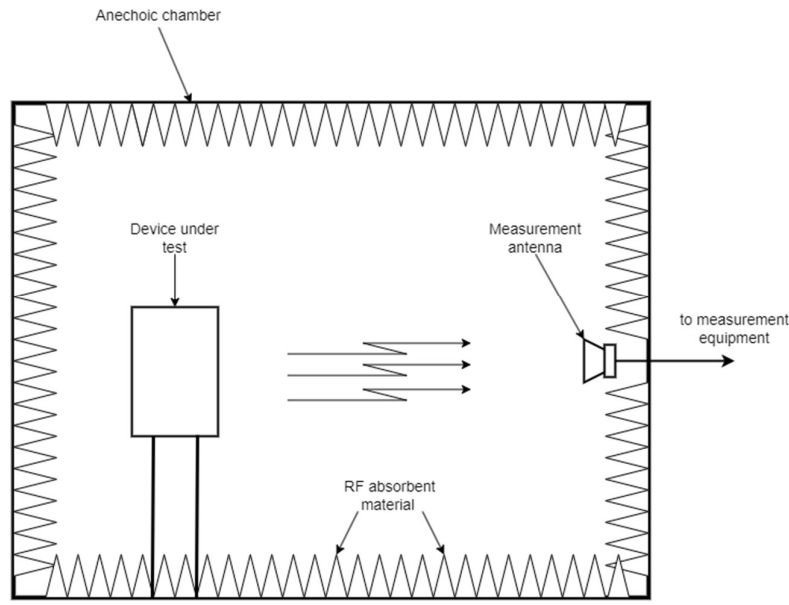


Figure 5: Graphical representation of a radio test setup within an anechoic chamber. The internal surfaces of the chamber are covered with RF absorbent material. The DUT is placed inside of the chamber and radiates radio signals during the test. Measurement antenna connected to measurement equipment, which are placed outside of the chamber.

An RF anechoic chamber is typically integrated within a screened room that is constructed using the Faraday cage principle. This is because many RF tests that necessitate an anechoic chamber to minimize the impact of reflections from the internal surfaces also require the characteristics of a screened room to weaken undesirable signals from entering and interfering with the equipment being tested, and also to prevent any emissions from the test setup to interfere with its external environment.

Since DUTs could have different characteristics, frequency bands and specific technology implemented, the maximum output RF power of the DUT may vary. However, the power rates can be considered as much higher than that of ambient RF sources because the former do not face obstacles, reflections, and other factors, which lead to loss of signal strength in the latter.

Therefore, considering the test approaches and test setups used in the telecom company, the following two sources of wasted energy have been identified: thermal energy and RF energy. Given the scope of this MSc thesis, only one EH solution could be further investigated. What follows describes the corresponding selection process.

3.2 Selection of a suitable energy harvesting method

Based on the sources of wasted energy accessible during test operations at the telecom company, the rest of this chapter gives the overview of EH methods applicable for energy harvesting from thermal and RF sources.

3.2.1 Thermal energy harvesting

TEGs can provide energy levels at the output in a range of nW to hundreds mW [31]. Standalone TEH devices are widely used in different applications such as aerospace, military, wearable devices or even in mobile communications systems [32]. TEH solutions are aimed at reusing the wasted heat from different sources, for instance produced by the human body, industrial machines, exhaust systems, etc. One of the main advantages of TEH application is that the heat sources are relatively constant; however, the available heat cannot be completely used and transformed to electrical energy [33], i.e., efficiency is limited.

Indeed, the efficiency of a TEH solution can be defined as the ratio between the electrical energy collected/stored to the total energy emitted. The overall output of the harvester depends on the total thermal energy [34], which could be applicable for different types of sensors and transmitters. The total output depends on temperature and area, but one of the main factors that influence the effectiveness of TEH is TEG's efficiency, which is limited to 5-15% [30]. Improving of the efficiency remains the main challenge nowadays. However, it is feasible to use TEH solutions for wearable devices (wristwatches, pulse oximeters, mobile devices, body sensors), supplied with electrical energy produced by human body heat [12].

In industrial applications, there exists an example of successful usage of TEH if the heat source emits high temperature (up to 1000 °C), in this case it is possible to harvest even kW of energy [35]. Although such temperatures are not reached in the case at hand at the telecom company, TEH is a promising approach that is further investigated in this thesis. A typical thermoelectric harvesting system consists of a TEG, a heat source, a cold source, and a DC-DC converter. When the heat source and cold source are applied on opposite sides of the TEG, a voltage appears at the output terminal, providing power to the load. A single TEG may generate power in a range from 1 to 125 W . More TEGs in parallel

and series could provide up to 5 kW; however, in this case the temperature difference between the heat and cold sources should be larger than 70°C [36].

The common diagram of the thermal EH solution as an example for self-powered wireless sensor network (WSN) is shown in Figure 6 [37].

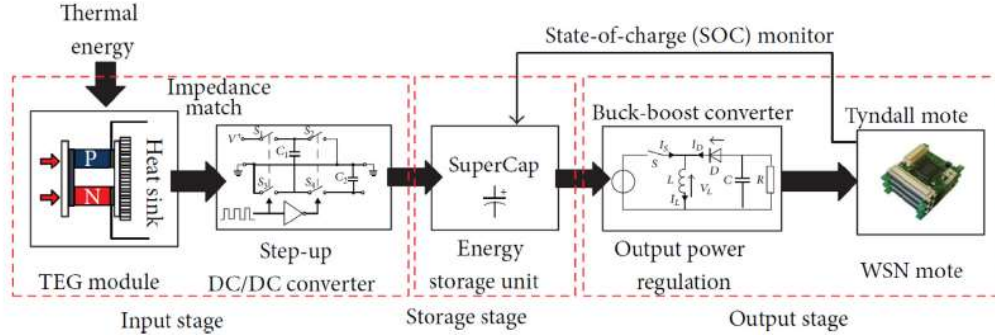


Figure 6: TEG diagram for self-powered application [37].

A TEG module is itself composed of thermoelectric couples, comprising a pair of P-type and N-type thermoelements (or legs), connected in series. The TEG generates electricity when a temperature gradient is applied. The larger the difference of the temperature $\Delta T = T_h - T_c$, the larger the power that can be collected at the output.

Next, the step-up DC-DC converter increases the output voltage from the TEG, to accurately control the output, which is necessary since the output voltage of the TEG is low and not constant [37]. Increasing the efficiency of the system could be achieved by implementing the Maximum Power Point Tracking (MPTT) algorithm.

The efficiency of thermoelectric EH solutions also depend on the thermocouples' metals, and there are several research efforts made for improving with usage of different metal pairs [13].

In the next stages, the energy is stored (in e.g., a supercapacitor) and then consumed by the load (e.g., active sensors).

3.2.2 RF energy harvesting

In comparison to other ambient energy sources, RF energy has a relatively low energy density of 0.2 nW/cm² to 1 μW/cm² [38].

There are two approaches that can be distinguished: 1) dedicated RF-EH and 2) ambient RF-EH. The dedicated approach means direct energy transfer between the energy source

and the harvesting device within a short distance; so, the harvesting device at short range is expected to produce power level within typically 50 nW/cm^2 [39].

It is feasible, for example, to power-on and sustain microcontrollers even using ambient digital-TV signals; the embedded wireless energy-harvesting prototype (E-WEHP) was able to power the sensing peripherals on a 16-bit PIC24F microcontroller at 6.3 km away from a TV tower [40].

The exponential growth of the mobile devices and their applications mean more base stations, towers and more radiating RF energy and more available sources. There is an abundance of RF energy and harvesting techniques that could provide alternative solutions for clean energy utilized in low power electronics application. However, to design an effective harvesting model, it is required to keep in mind the spectrum properties of the RF source, i.e., a system should be able to absorb a certain band range of frequency [41].

In urban and semi-urban environments, the ambient multi-band (GSM 900/1800, 3G, DTV) RF-EH solutions could represent high efficiency up to 40% measured in a controlled environment [42].

Some researchers have conducted experiments with different antenna types and rectifiers combined into RF-EH solution. They were able to estimate that antenna type and polarization, as well as designing for a specific frequency band influence the RF-EH solution effectiveness. An experiment has shown that a duck antenna¹ had the most effective result and resulted in a voltage output of 780 mV [43].

Most of the RF-EH solutions existing and researched at the moment consist of some common components: receiving antenna, RF-DC converter (rectifier) and load or energy storage. The most common definition of the main segment of RF-EH is *rectenna*, which is a combination of antenna and rectifier. The common diagram is shown in Figure 7 [44]

¹ A duck antenna (rubber ducky antenna) is a flexible antenna used on e.g., portable handheld radios and resembles a rubber duck or duckbill.

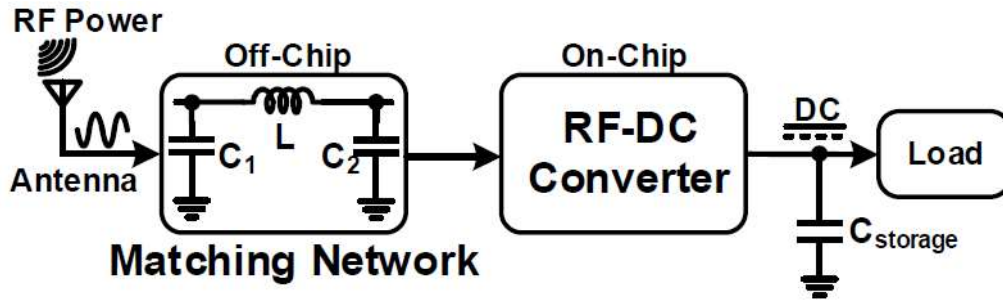


Figure 7: Block diagram of RF-EH Solution [44].

An RF energy harvesting solution is very demanding to antenna design, antenna polarization, and depends on the frequency band.

The antenna array could be designed for wideband and hybrid feeding network. The following bands are popular sources in the ambient RF harvesting: GSM900/1800, 1800/4G, UMTS 2100/3G, LTE/NR 2600/4G/5G. For those bands (900 to 2600MHz) the proper antenna design could eliminate gaps in RF-DC rectifier implementation and increase efficiency of the harvesting solution. The experimental antenna designed to prove this concept and the measurements showed that with proper antenna positioning the maximum recorded voltage in ambient environment in 70 m from the base station was 194.5 mV, corresponding to 47 μ W power [45].

Specifically, for GSM900/1800, 3G, and 4G, a patented RF-EH solution exists [46]. The apparatus consists of antenna component, designed specifically for respective band, filter and rectifier for levels under 3 μ W.

Rectification circuit design exists in different implementations. A commonly used approach is a power amplifier circuit that yields enough DC energy from the environment. Those rectifiers are quite simple, and as a basic implementation they are done as a combination of full-wave rectifier with a voltage multiplier. Depending on the purpose of certain RF harvesting solution, the optimization of the rectifier module becomes the main issue to solve [5].

Rectifier optimization and enhancement is aimed at increasing RF-DC efficiency and limit the usage for a particular application. Opposite to antenna implementation principles

(wideband, hybrid feeding source), the rectifier efficiency increases if it is limited to work for certain restricted frequency band. There are high demanding requirements to RF-DC rectifiers, since they are aimed at working within very low power conditions and reducing the power leakage. One of the optimization approaches uses a threshold voltage cancellation scheme; with this the efficiency of the rectifier improved to 38-39% depending on the load [47].

There are several optimized rectifier schemes available for analysis and tests. Another example is a combination of several techniques of threshold voltage cancellation and the technique of cascade arrangement to improve the output voltage [48].

This chapter outlined available wasted energy sources at the telecom company during testing operations by describing the test process, equipment, and approach. Thermal and RF EH methods are considered as suitable approaches for the telecom company. Those methods were analyzed and described more thoroughly, including main working principles, approximate power ratings estimations and typical implementation techniques. However, considering the specificities of the measurement procedures in testing processes, it was found out that the RF EH method is not suitable because introducing rectenna, RF-DC rectifiers or any similar electronics circuits may affect the measurement results during test executions.

On the other hand, the thermal energy harvesting method does not suffer from this and therefore it is selected as the only applicable technique for further development, investigation, and experiments in this MSc thesis.

The corresponding design, implementation, and experiments are presented in the next chapters.

4 Developed thermal energy generator hardware solution and simulation results

This chapter describes the development of the thermal energy EH solution, including design, implementation, and estimation of the main parameters. It gives an overview of the main components, their working principles, and the simulation results.

4.1 Design

The proposed TEH consists of two parts: 1) A TEG (See Section 4.2.1) and 2) a DC-DC integrated converter (see Section 4.2.3).

Before presenting the actual implementation with exact references of the components, let's consider the TEG design principle.

The main goal is to design a minimum viable device to verify the thermal energy harvester properties. The proposed TEG has dimensions $250*165*1.5$ mm. These dimensions were selected for several reasons, notably to make the TEG lightweight, versatile for different DUTs, and attachable to different heat sources.

The proposed solution consists of a Peltier elements array. A Peltier element, also known as a thermoelectric cooler or TEC, consists of a set of thermocouples, connected in series. Typically, a TEC is made of bismuth telluride (Bi_2Te_3) that are sandwiched together between two metal plates. When a DC current is applied to the element, electrons flow from the hot side to the cold side, which results in a heat transfer from one side of the element to another. This principle is commonly used in small refrigerators and coolers [33]. However, due to the Seebeck effect [10], applying temperature difference to Peltier device surfaces will result in a current flowing through the load resistance of the device. The Seebeck effect occurs because the flow of electrons in a conductor or semiconductor is affected by temperature. When two conductors made of different materials are connected at different temperatures, electrons flow from the hotter material to the cooler material, generating a voltage difference between the two ends. Figure 8 illustrates both principles – refrigeration mode (“Peltier effect”) and power-generation mode (“Seebeck effect”).

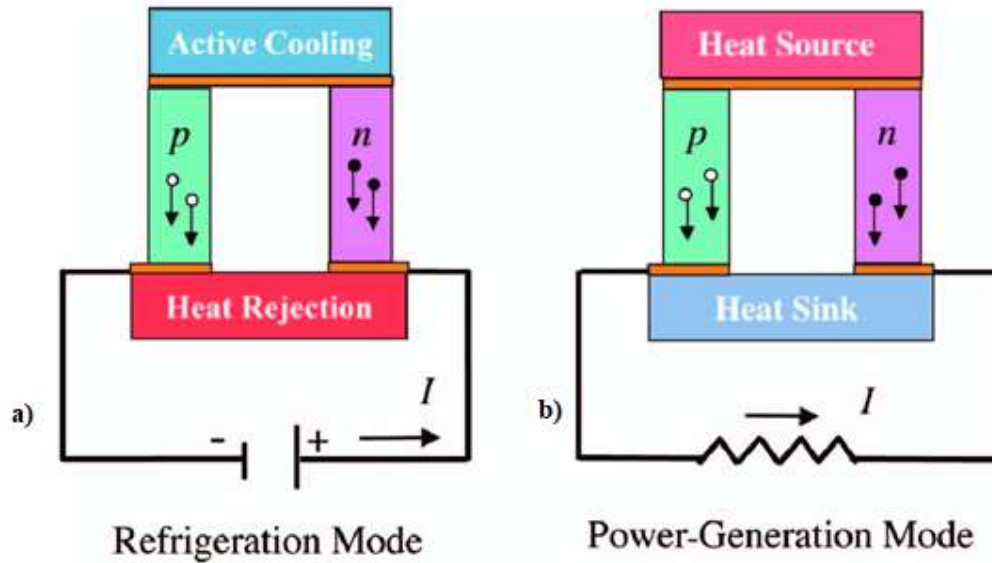


Figure 8: Schematic diagram of Peltier thermoelectric couple, consisting of n-type and p-type thermoelectric materials [49] : a) refrigeration mode when the current I applied to the Peltier element input and b) power-generation mode, when the current I generated on Peltier element inputs if temperature difference applied to the Peltier element surfaces.

Typically, a Peltier element consists of thermocouples array distributed in different form factors, varying in size, shapes, and number of layers. TEC characteristics also may vary and include maximum operating temperature, maximum temperature difference across the TEC, maximum voltage, and current ratings.

For the case at hand, taking into consideration the maximum temperature ratings, which includes measured maximum temperature of available source $T_{max} = 60^{\circ}\text{C}$ with ambient temperature $T_{ambient} = 25^{\circ}\text{C}$, meaning $\Delta T = 35^{\circ}\text{C}$, a standard Peltier element ATS-TEC40-39-004 with $\Delta T_{max} = 68^{\circ}\text{C}$ and 127 thermocouples in its assembly [50] was selected for the developed solution. Therefore, the developed TEG assembly can accommodate and actually consists of 15 Peltier elements, where each element has dimensions $40 \times 40 \text{ mm}$ and the distance between the elements is approximately 5 mm .

To increase the output characteristics of the TEG, a heatsink is required to be installed on the cold side of the TEG to achieve a larger constant ΔT , since this parameter is a key to output voltage. Detailed calculation and parameters estimation are given in Section 4.2.2.

4.2 Implementation

As mentioned previously, the TEH solution consists of the TEG itself as well as an output stabilization and conversion module; this section focuses on both parts more thoroughly from an implementation perspective.

4.2.1 Proposed TEG

The proposed TEG is designed as an array of 15 Peltier elements, organized as 3 rows of 5 elements. In order to distribute heat between the elements evenly, the elements array is affixed to an aluminium plate with dimensions 250*165*1.5 mm and adhered with thermal conductive glue. For better thermal isolation of hot and cold parts of the TEG, the elements are placed with gaps to reduce mutual elements heating. The distance between the elements is approximately 5 mm. Gaps between the elements are filled with thermal isolation silicone.

The cold side of the TEG consists of 15 heat sinks, adhered to Peltier elements with thermal conductive glue.

Thus, this approach allows providing better isolation between hot and cold sides of the TEG, reduce mutual elements heating and diminish the effect of thermal transfer between the hot and cold sides. An illustration of the TEG assembly (side view) is show in Figure 9, and the corresponding physical prototype assembly is shown in Figure 10.

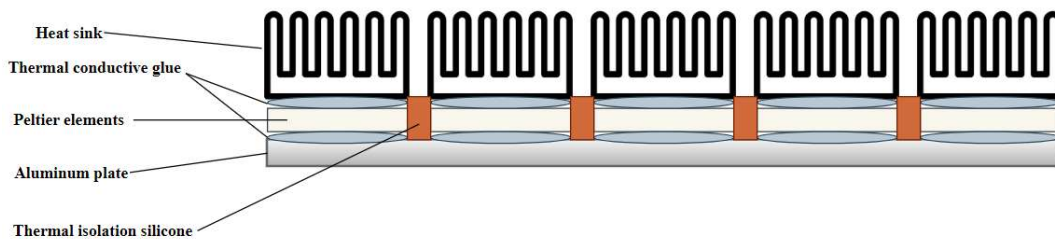


Figure 9: Proposed TEG assembly illustration (side view, corresponding to 1 row of 5 Peltier elements).



Figure 10: Photograph of the initial developed prototype TEG assembly with 15 Peltier elements for the proposed TEG. Notice that the elements are not connected, which allows testing different configurations of series and parallel connections.

In Figure 10 it can be seen that the Peltier elements are not interconnected, as the total performance of TEG depends on connection diagram between elements; so, the set of experiments described in Chapter 5 consider different configurations of series and parallel connections to estimate the corresponding power and effectiveness output characteristics.

4.2.2 TEG output parameters and effectiveness estimation

Each element used in the assembly consists of 127 thermocouples made from bismuth telluride (Bi_2Te_3) and with Seebeck coefficient $S_{AB} = 200 \times 10^{-6} \text{ V}/^\circ\text{K}$. The maximum output of the single TEG can be calculated with Equation (1):

$$V_{out} = N \cdot \alpha_{AB} \cdot \Delta T \quad (1)$$

where N is the number of connected thermocouples, α_{AB} is the Seebeck coefficients of the two joined materials A and B forming the thermocouple, and which can be derived as per Equation (2):

$$\alpha_{AB} = \alpha_A - \alpha_B \quad (2)$$

As the maximum temperature source available is $T_{max} = 60 \text{ }^\circ\text{C}$ with ambient temperature $T_{ambient} = 25 \text{ }^\circ\text{C}$, so $\Delta T = 35 \text{ }^\circ\text{C}$. In this case, the maximum estimated output voltage per element is estimated as $V_{TEC_out} = 0.889 \text{ V}$ as per Equation (1). Figure 11 shows the dependency between the temperature difference applied to the TEC and the corresponding estimated output voltage.

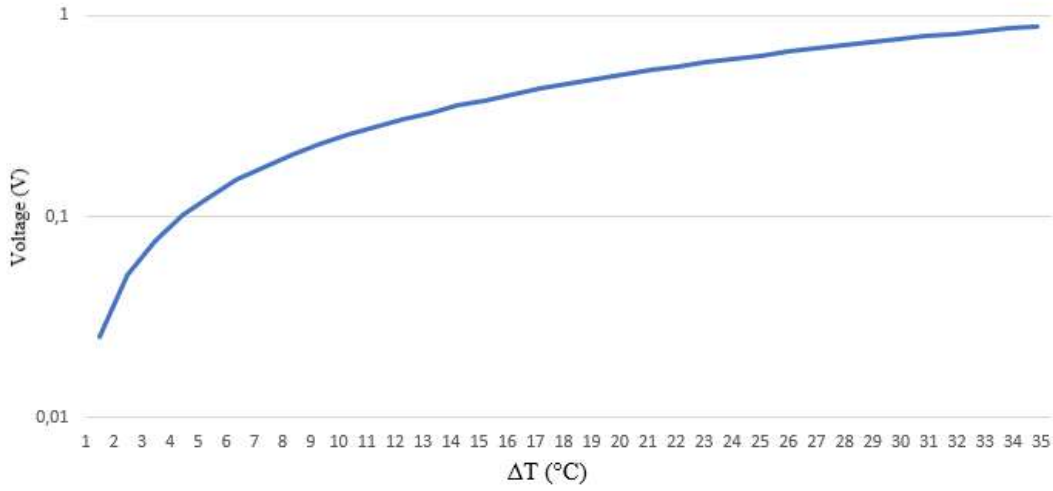


Figure 11: Estimated output voltage V of the single TEC depending on temperature difference ΔT ($^\circ\text{C}$).

The maximum output current I is determined by Equation (3):

$$I = \frac{V_{out}}{R_L + R_g} \quad (3)$$

where R_L is the load resistance and R_g is the internal resistance of the Peltier element. According to Peltier element datasheet [50], the internal resistance of the module is $R_g = 2.05 \text{ } \Omega$. The maximum power output could be calculated using Equation (4):

$$P_{out\ max} = \frac{V_{out}^2}{4R_{total}} \quad (4)$$

where $R_{total} = R_L + R_g$.

The TEG effectiveness and material appropriateness can be expressed through the dimensionless figure of merit (FOM), ZT [51], and expressed with Equation (5):

$$ZT = \frac{\alpha^2 T}{\rho \lambda} \quad (5)$$

where α is the Seebeck coefficient, T is the absolute temperature, ρ is the electrical resistivity and λ is the thermal conductivity of the material. The figure of merit allows to calculate the efficiency of a thermoelectric material during the conversion of the heat into electricity. The maximum efficiency of a thermoelectric power generator operating as a reversible heat engine is limited by the second law of thermodynamics [52]; it is known as the Carnot efficiency and can be expressed with Equation (6):

$$\eta_{Carnot} = 1 - \frac{T_c}{T_h} \quad (6)$$

where T_c is the temperature on the cold side of the TEG and T_h in the temperature at the hot side of the TEG.

Therefore, the total maximum effectiveness of the TEG can be calculated with Equation (7):

$$\eta_{max} = \frac{T_h - T_c}{T_h} \frac{\sqrt{1 + ZT} - 1}{\sqrt{1 + ZT} + \frac{T_c}{T_h}} \quad (7)$$

Given of the above, the ideal effectiveness η_{max} (%) for a bismuth telluride based TEG at operating temperature range between 25 °C and 60 °C can be estimated as per the curve shown in Figure 12.

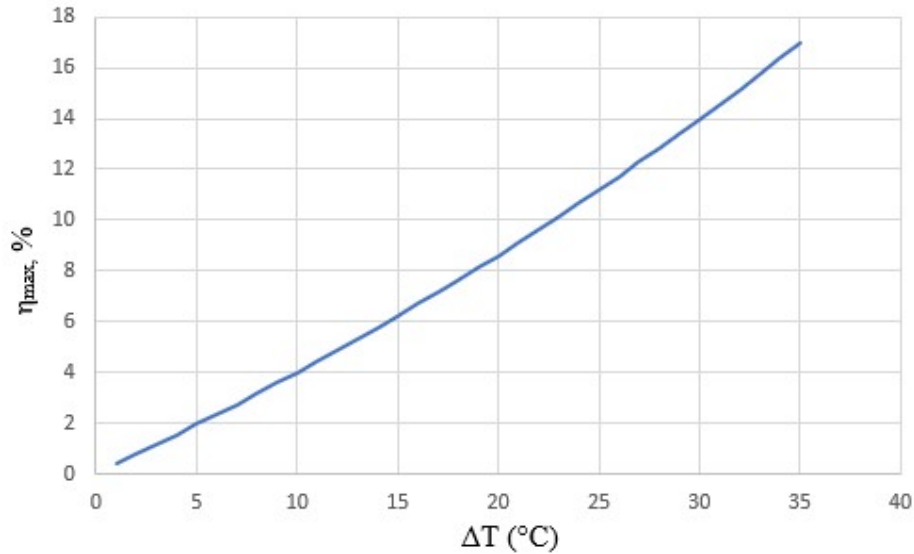


Figure 12: Bismuth telluride based TEG's effectiveness estimation η_{max} (%), depending on temperature difference between the hot and cold sides ΔT (°C).

However, for bismuth telluride the conventional equations have limitations due to the fact that thermoelectric parameters change with temperature; so, the figure of merit and the effectiveness of the TEG changes with temperature as well [53]. In theory, the efficiency increases as the temperature difference between the cold and hot sides increases. In ideal conditions, the average efficiency increases from 2% at temperature gradient of 25 °C to 11.5% at temperature gradient of 230 °C, and this dependency is non-linear [54]. However, in practical experiments it is expected to observe lower efficiency due to temperature losses and parasitic losses through the TEG elements connections and junctions.

The above assumptions are tested experimentally and described in more details in Chapter 5.

4.2.3 TEG output conversion

The output of the TEG is not stable as it can change depending on the temperature gradient and the mutual heating of the hot and cold sides. Another disadvantage of the TEG assembly is that the output decreases over time: after the heat sink warms up, the temperature gradient decreases, which in turn decreases the output voltage. Thus, the output voltage should be boosted and stabilized.

The conventional approach is to use a Maximum Power Point Tracking (MPPT) converter; however, it is hard to determine the maximum power point for a TEG since the output depends on many factors [55]. Nowadays, there is a wide range of DC-DC converters in the form of integrated circuits available on the market and could be used for boosting and stabilizing the output of energy harvesters.

As the TEG estimate output power levels are relatively low, the selection of the DC-DC converter comes down to its input voltage range and its capabilities. To simplify the implementation of the power conditioning circuit for energy harvesting applications, the commercial Integrated Circuit LTC3108 [56] from Linear Technology was selected. This integrated solution contains all the necessary components for the power conditioning circuit. The step-up regulator is based on a synchronous boost converter with Armstrong's oscillator, using a transformer with a turn ratio of 1:100. The output voltage of the regulator can be programmed to 2.5 V, 3 V, 3.7 V, or 5 V. The LTC3108 is a step-up regulator-integrated circuit that requires an input voltage as low as 20 mV. Having this in mind, for experimental purposes in this thesis, the LTC3108 has been selected as it shows the most suitable characteristics for thermal energy harvesting [55].

Let's review the typical application of LTC3108 block diagram. The transformer, MOSFET and capacitor C2 are forming a step-up oscillator, which allows to start up with a 20 mV across V_{in} input from a TEG. The input is drawn through capacitor C1, rectified, and filtered out to the V_{aux} output. When the V_{aux} voltage reaches 2.5 V, a charge control module switches on and activates the V_{out} output. Along with that, the programmable voltage VS1 and VS2 start operating, so it could be set to values 2.5 V, 3 V, 3.7 V, or 5 V. Separate output V_{LDO} allows to get a low dropout (LDO) regulated at 2.2 V, which turns on quicker than V_{out} ; so once the V_{aux} reaches 2.3 V, the V_{LDO} will be active, which allows to use it before V_{out} . There is also separate voltage outputs V_{out2} and V_{out2_en} with a MOSFET switch, so it is possible to feed a signal to V_{out2_en} , limited to 300 mA and enable output at V_{out2} . V_{store} output intended to be used as a storage output and is connected through the MOSFET from V_{aux} and switches on by charge control. It allows to connect V_{store} to supercapacitor or any other storage capacitor. Once the input from the TEG becomes low, and V_{out} charge control switches off too, the voltage at V_{out} will be still available until C_{STORE} capacitor has charge. A typical LTC3108 application diagram is shown in Figure 13. The corresponding assembled circuit is shown in Figure 14.

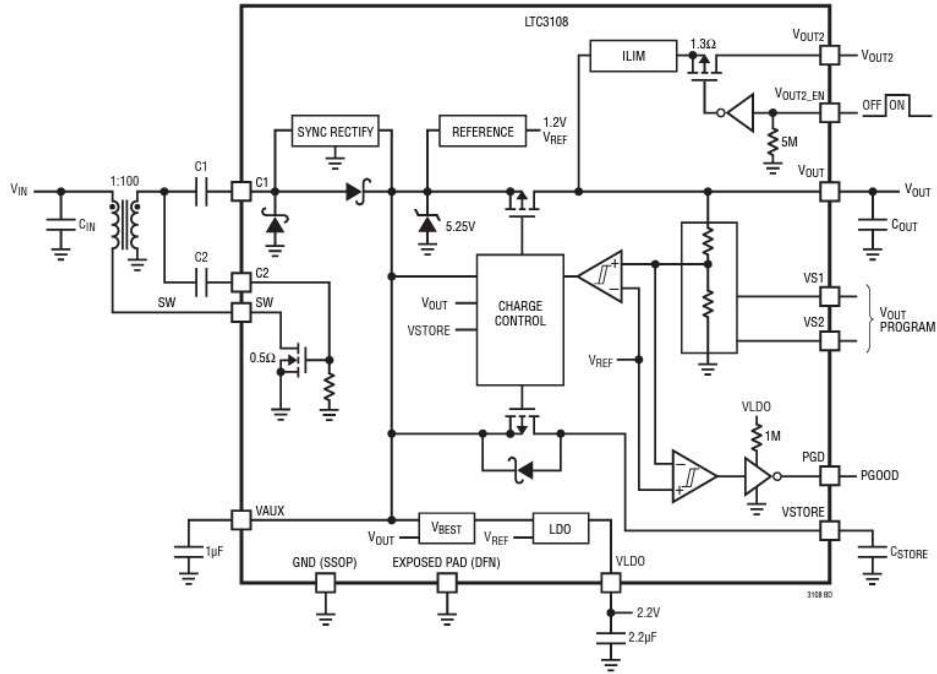


Figure 13: LTC3108 block diagram for a typical application [56].

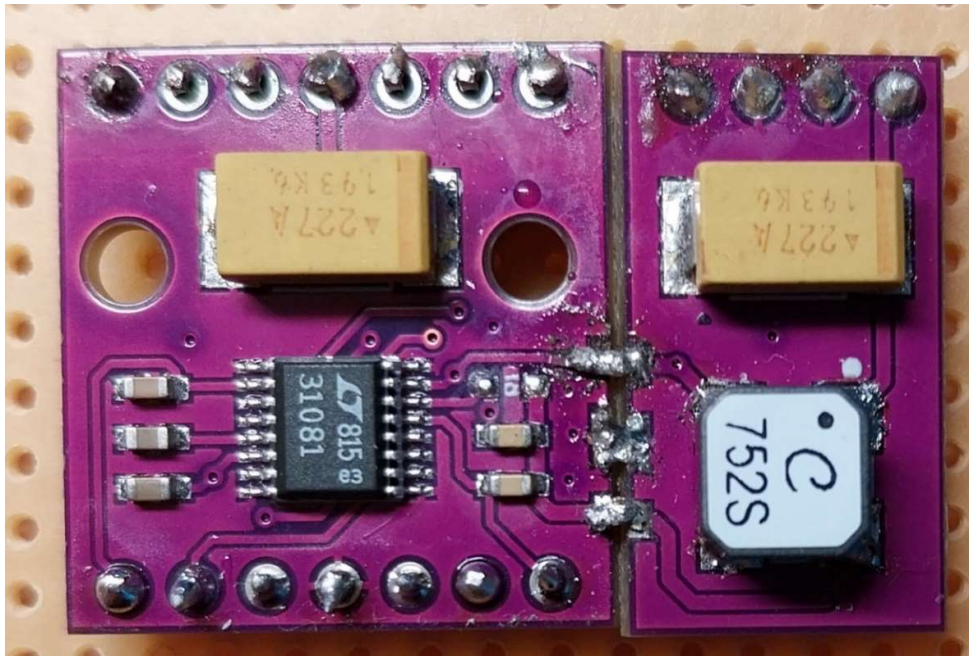


Figure 14: The assembled circuit for LTC3108 (marked LTC3108) and external components (transformer and capacitors)

To estimate and analyze the expected properties of this circuit, SPICE simulations were conducted with equivalent schematics and different input parameters, as described in what follows.

4.2.4 SPICE simulation results

To implement the schematics for simulation it is required to use a simulation software; LTSpice by Analog Devices company was used for this purpose. The main goal of the simulation is to estimate the output parameters of the DC converter circuit when TEG output is connected to converter input. The TEG output is simulated as an equivalent voltage source with variable voltage output per time.

The equivalent schematics of the assembled DC converter circuit is shown in Figure 15.

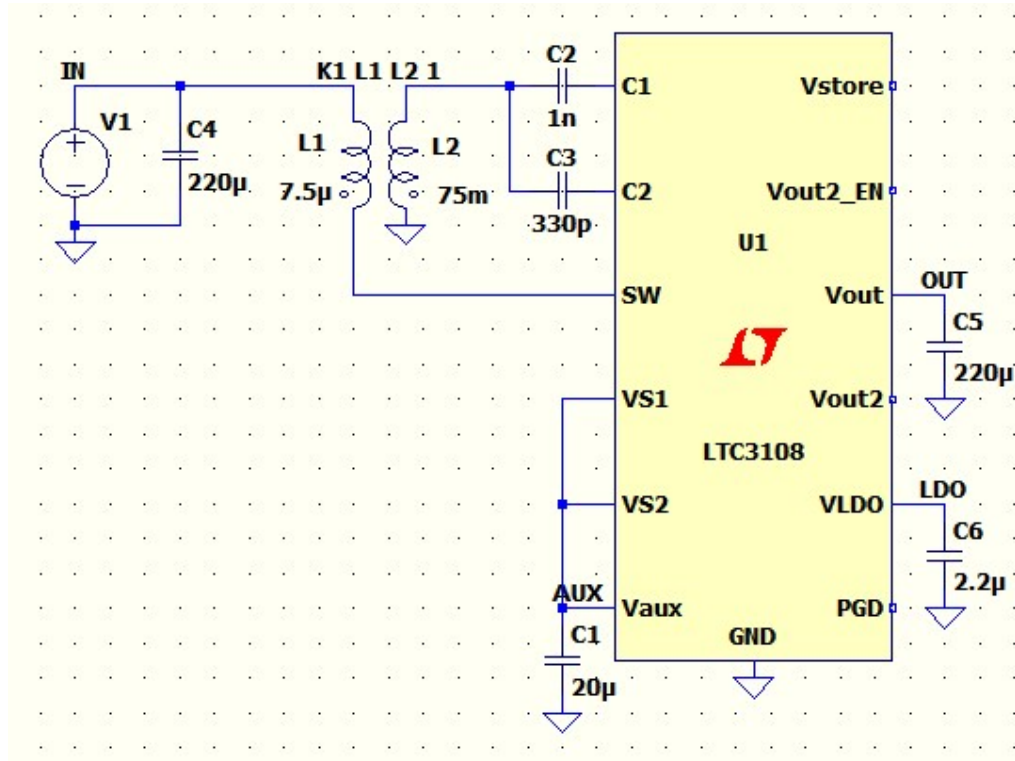


Figure 15: Equivalent schematics of the assembled DC converter circuit for LTC3108 for simulation purposes.

For the first round of simulation, let's consider the single TEG with output parameters, corresponding the estimated output voltage, shown in Figure 11 in Section 4.2.2. TEG output simulation is performed using piecewise linear (PWL) function, which allows to construct a waveform consisting of a series of different DC voltages.

The first goal is to check the DC converter output at V_{LDO} , V_{aux} and V_{out} to verify the working principle of the LTC3108, described in Section 4.2.3. The following simulations are considered to verify charge control and output parameters. The programmable output of VS1 and VS2 are set to enable maximum output voltage V_{out} to be equal to 5 V. Additionally, V_{store} is not the subject of simulation and experiments since the focus is to validate the maximum output parameters of the DC converter. Energy storage is not considered as part of the subject for simulations and experiments.

First simulation is performed during 1 s and the TEG output voltage range is 0.01 – 1 V. The simulation output result is shown in Figure 16. In this figure, the output from the TEG is the input to DC converter and represented on the chart by the purple line “V(in)”, V_{aux} is represented with the green line and labelled “V(aux)”, V_{LDO} is represented with the brown line and labelled as “V(ldo)”, and finally V_{out} is represented with the blue line and labelled “V(out)”.

As can be seen from the simulation results, once V_{aux} reaches 2.5 V, and charge control switches on, V_{LDO} starts operating. As expected, V_{out} starts operating as well and reaches 2.5 V. In turn, since the input of the DC converter continue increasing, V_{aux} reaches its maximum to 5.2 V. V_{out} reaches 5 V as programmed.

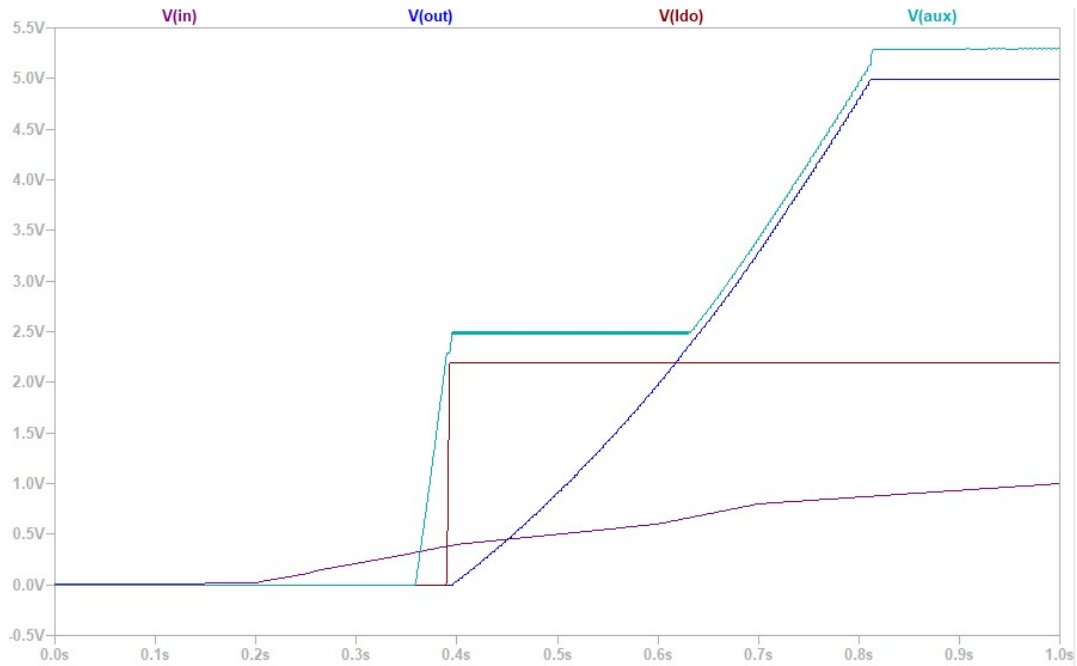


Figure 16: SPICE simulation results for LTC3108 DC converter with input increase from 0.01V to 1V during 1 s. The input voltage V_{in} is shown with the purple line on the chart, the output voltage V_{out} with the blue line, and V_{LDO} with the brown line and V_{aux} with the green line.

The simulation results confirm the main working principles of the DC converter, described in Section 4.2.3, and works as expected.

The next simulation goal is to verify that the output of the DC converter will remain stable when the TEG performance and output voltage decrease. It is expected that the TEG hot side will influence the cold side, so ΔT will decrease due to mutual heating, so the output of the TEG will decrease as well. The actual voltage parameters of the TEG are verified in Chapter 5; however, it is possible to estimate its output, and verify what is the minimum ΔT is required to keep the DC output stable. To do that, the PWL function is constructed to simulate the TEG output from its estimated maximum for $\Delta T = 35\text{ }^{\circ}\text{C}$ with corresponding theoretical TEG output $V_{TEG_out} = 0.889\text{ V}$. The minimum input voltage for DC converter is 0.02 V , which corresponds to $\Delta T = 1\text{ }^{\circ}\text{C}$ for a single TEG, as per Equation (1). Therefore, the PWL function is constructed as a set of voltages in the range from 0.889 V to 0.02 V decreasing during 1 s and remains at the level of 0.02 V during the next 3 s . Simulation results are shown in Figure 17.

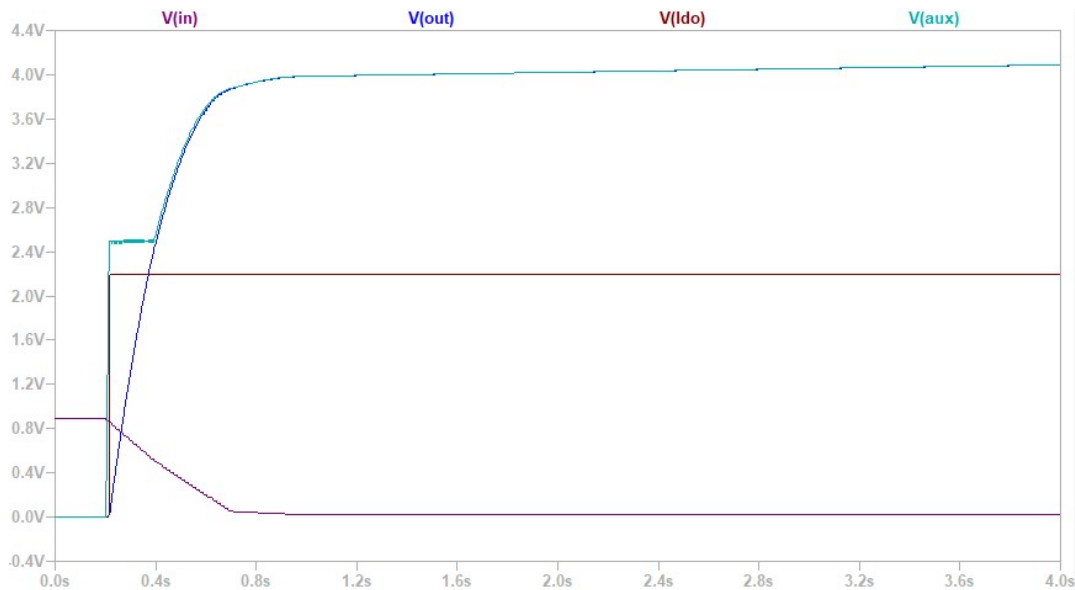


Figure 17: SPICE simulation result for LTC3108 DC converter with input decrease from 0.889 V to 0.02 V during 1 s and keep the input at 0.02 V during next 3 s . V_{in} is shown with a purple line on the chart, V_{out} with the blue line, and VLDO with the brown line and V_{aux} with the green line.

As can be seen from the simulation result, V_{aux} (represented with the green line and labelled as “ V_{aux} ”) reaches a maximum of 4 V within approximately 1 s and remains stable over the rest of simulation time. V_{out} (blue line on the chart, labelled as “ V_{out} ”)

could not reach the maximum of 5 V and stays at the level of 4 V; V_{LDO} (brown line on the chart labelled as “V(ldo)”) remains stable during whole simulation.

Additionally, for this simulation the PWL function constructed to check the minimum output of the TEG $V_{TEC_out} = 0.01 V$, which corresponds to $\Delta T < 1 \text{ }^\circ\text{C}$ to verify if the voltages at the DC converter outputs will drop when DC converter input drops lower than $V_{in} = 0.02 V$.

To do that, the PWL function was designed in such a way that the voltage drops over the first 1 s from 0.889 V to 0.02 V and then continue dropping to 0.01 V during next 3 s, as shown in Figure 18.

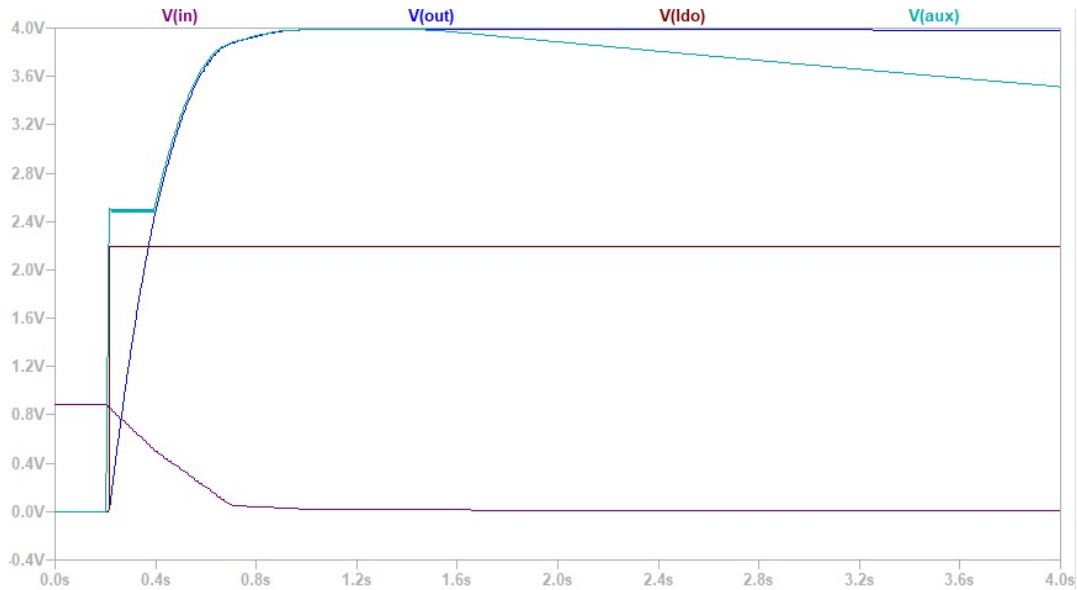


Figure 18: SPICE simulation result for LTC3108 DC converter with input decrease from 0.889V to 0.02V during 1 s and drops further during the next 3 s to 0.01V. V_{in} is shown with the purple line on the chart, V_{out} with the blue line, and V_{LDO} with the brown line and V_{aux} with the green line.

As visible from the simulation results, V_{aux} output voltage (green line on the chart, labelled as “V(aux)”) reaches 4 V and starts to decrease at the time of 1.6 s. V_{out} cannot reach its maximum and remains at the level of 4 V. When V_{in} voltage (purple line on the chart, labelled as “V(in)”) becomes lower than 0.02 V, V_{out} (blue line, labelled as “V(out)”) remains at the level of 4 V and V_{LDO} (brown line on the chart, labelled “V(ldo)”) remains stable at the level of 2.2 V. In comparison to the previous result, because of the input voltage is lower than 0.02 V, V_{aux} is decreasing.

Since the designed TEG consists of 15 Peltier elements, it could be expected that the maximum output voltage of the TEG could be reached if elements are connected in series

and at the maximum $\Delta T = 35\text{ }^{\circ}\text{C}$ the total maximum output of the whole assembly could be estimated as $V_{\text{TEG_out_max}} = 13.335\text{ V}$. In this case it is not recommended to operate the DC converter with this voltage output, as the maximum input voltage for C1 and C2 inputs may vary in a range of 2 V to 8 V at peak during shorten amount of time [55]. Therefore, in this particular case it is a restriction for DC converter usage, although, due to mutual heating of elements and non-stable ΔT , it is expected that the TEG will not reach its maximum estimated output.

This chapter has presented the proposed TEG design, calculation of maximum TEG output parameters and effectiveness estimation, main working principles of the DC converter and simulation results, and its usage restrictions. The next chapter presents the real-life experiments with the developed TEG.

5 Real-life experiments

This chapter describes the real-life experiments with the TEG, including the output and effectiveness parameters measurements, as well as experiments with the output conversion module. The goal of this series of experiments is to understand how the TEG operational principle, dependability on thermal parameters of the heat source and the electrical output. The experiments are also aimed at finding the maximum electrical output of the TEG by testing varies connection schematics of the Peltier elements of the TEG. Additionally, another goal is to verify the DC converter operation principles previously described and simulated in Sections 4.2.3 and 4.2.4.

5.1 Testing of the TEG

To start the experiments, the heat source temperature range was measured. A radio equipment DUT during the load testing process was acting as a heat source. To measure the DUT temperature, the load test has been executed and the temperature was measured with a distance thermometer (pyrometer). The test was executed for 40 min; the temperature measurements are shown on Figure 19.

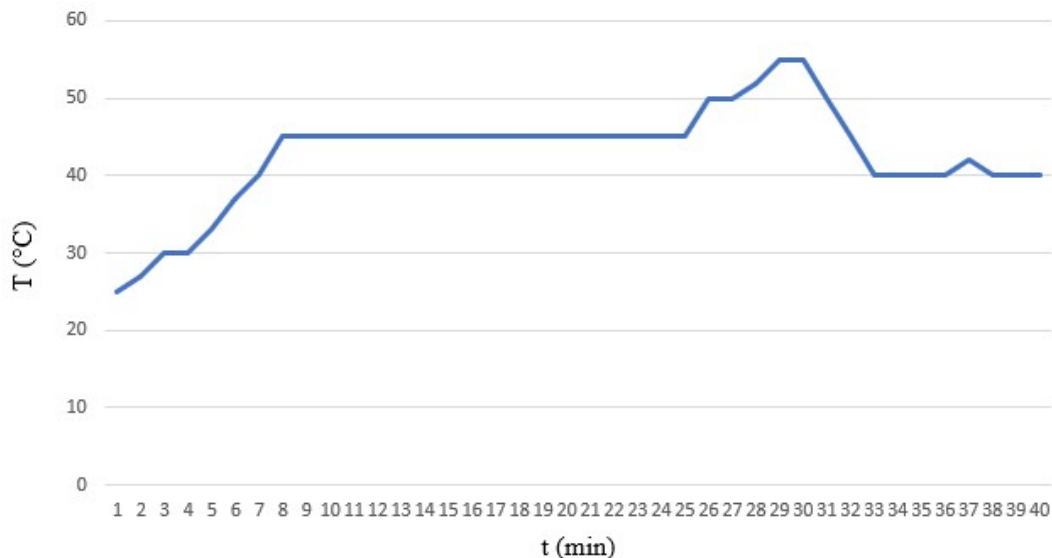


Figure 19: Radio equipment DUT temperature T (°C) measurements during load test during test execution time t (min).

As seen from the temperature measurements, the temperature is raising during the first 9 min, then becomes stable during next 14 min, then raises to 55 °C for 2 min, then drops to 40 °C at $t = 33$ min and finally remains stable until the end of the test execution. Therefore, since $T_{\text{ambient}} = 25$ °C, the measured ΔT falls into the range 0 – 30 °C during the test execution time. Figure 20 illustrates the ΔT (°C) values during the test execution time t (min).

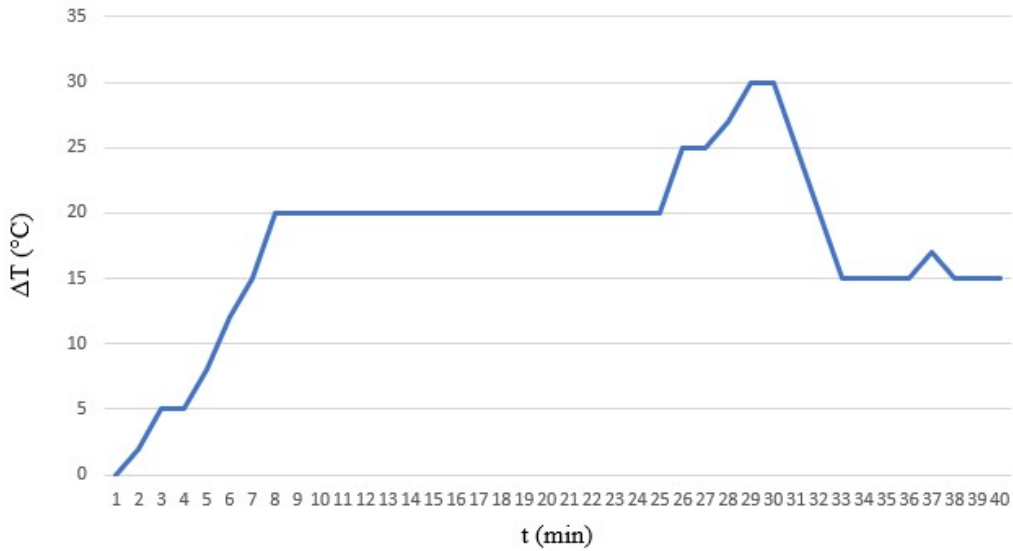


Figure 20: Temperature difference ΔT (°C) during test execution time t (min).

As can be seen from Figure 20, the maximum ΔT (°C) reaches its maximum of 30 °C for 2 min, but during most of the test execution time it remains stable at 20 °C.

Next, to start experimenting with the TEG, first the TEG elements were connected in series to reach the maximum voltage output. Figure 21 shows the corresponding connection schematics of Peltier elements on the TEG.

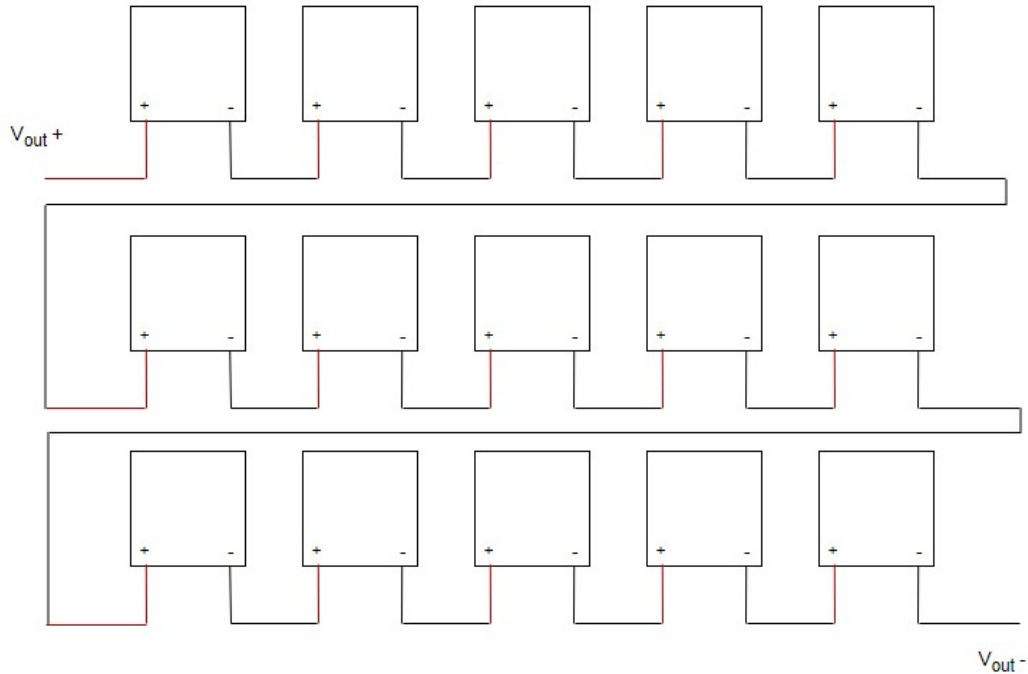


Figure 21: Schematic representation of proposed TEG connection diagram (all Peltier elements connected in series) for achieving the maximum voltage output.

The TEG assembly hot side was attached to the surface of the DUT before the test was executed. A multimeter (Fluke F15b+) was used to measure the voltage output of the TEG and connected to V_{out+} and V_{out-} TEG outputs (shown in Figure 21). Then the load test was executed.

During the test execution time, the following parameters were measured: voltage and current output of the TEG assembly, temperature difference of DUT surface and ambient temperature, temperature difference of DUT surface (TEG hot side), and TEG cold side (heat sinks).

As expected, the temperature difference between the TEG hot and cold sides is lower than the temperature difference between the DUT surface and ambient temperature since the TEG surfaces undergo a mutual heating and thermal conduction between the hot and cold sides. Therefore, the output voltage of the TEG is much smaller that it was estimated theoretically, reaching 3.5 V at its maximum and dropping to 0.7 V at its minimum. The TEG temperature difference between the cold and hot sides were measured in a range of 9.2 °C at maximum and 1.83 °C at minimum. The temperature and output voltage measurements are shown in Figure 22.

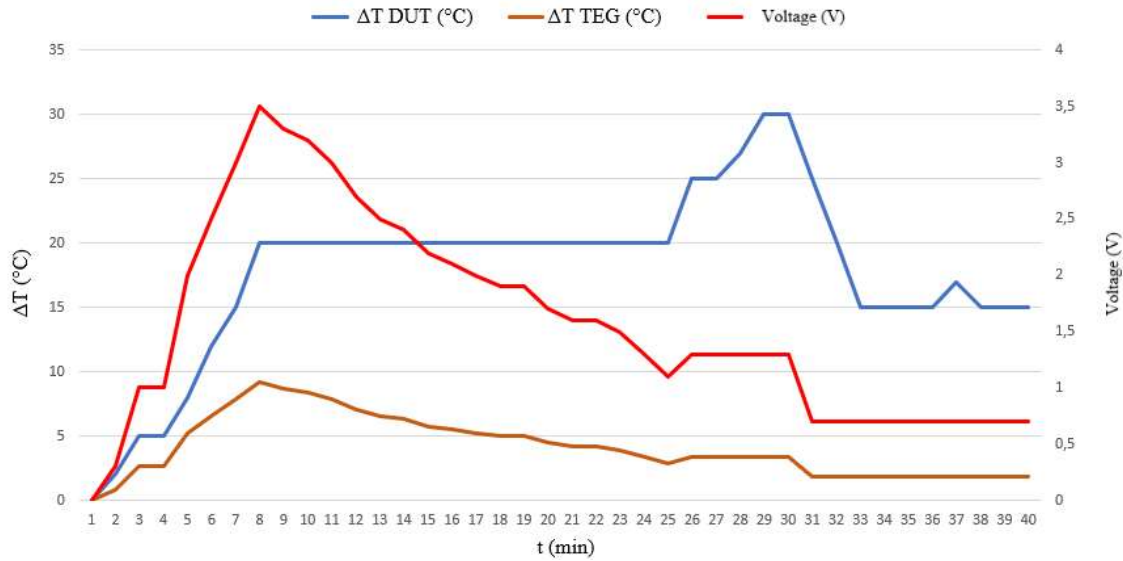


Figure 22: Measurement results with all Peltier elements connected in series for achieving the maximum voltage output (schematic of Figure 21): measured voltage output Voltage (V) of the TEG (red line), temperature difference of the DUT surface and ambient temperature ΔT (°C) (blue line), and temperature difference between the hot and cold sides of the TEG ΔT (°C) (brown line).

The experiment and measurements show that the maximum temperature difference ΔT cannot be reached on the TEG surfaces, so the total voltage output could not reach the estimated theoretical maximum. The maximum current output was measured at the level of 0.12 A and the minimum at 0.02 A. Therefore, the total maximum power $P_{\text{TEG_out}}$ is in the range of 0.014 – 0.42 W.

The goal of the next experiment is to increase the current output $I_{\text{TEG_max}}$ of the TEG by connecting the 3 rows of Peltier elements in parallel, and the 5 elements in each row in series. Figure 23 represents the corresponding connection schematics of Peltier elements on the TEG.

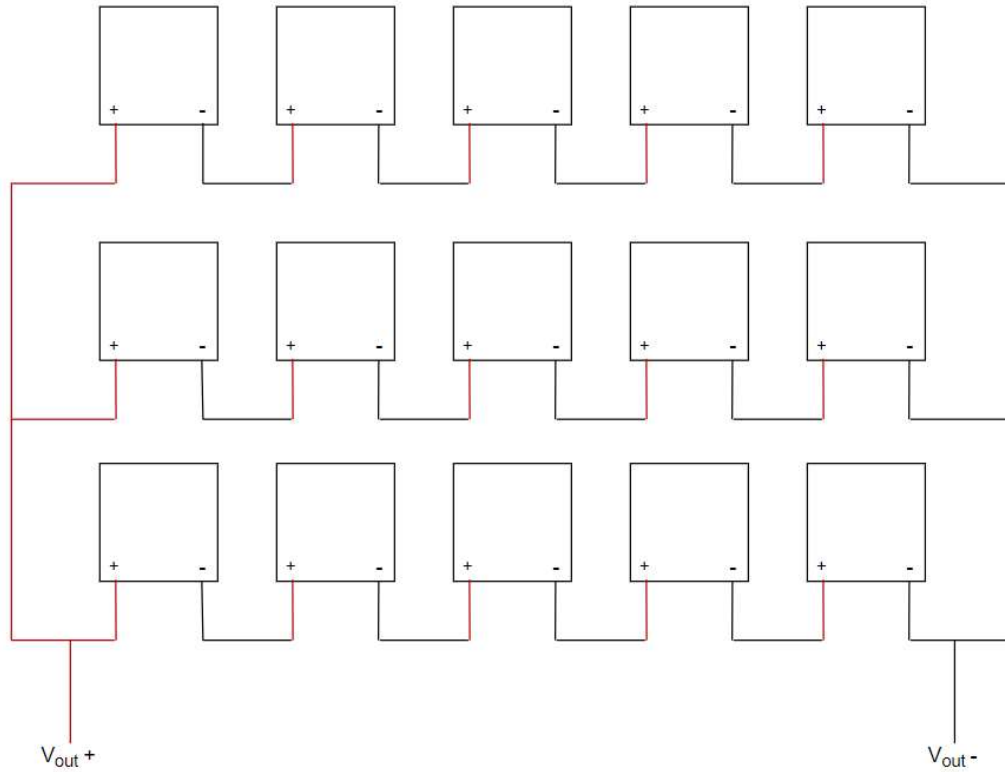


Figure 23: Schematic representation of proposed TEG connection diagram for the purpose of increasing the current output I_{TEG_max} ; The Peltier elements are organized as 3 rows wherein the 5 elements connected in series. The rows are connected in parallel.

The TEG and DUT were cooled down after the first experiment, then the assembly's hot side was attached to the surface of the DUT before the test was executed. The multimeter was used to measure the voltage output of the TEG and connected to V_{out+} and V_{out-} . TEG outputs (shown in Figure 23). Then the load test was executed again.

During the experiment, same parameters were measured as in the previous experiment, i.e., voltage and current output of the TEG assembly, temperature difference of DUT surface and ambient temperature, temperature difference of DUT surface (TEG hot side) and TEG cold side (heat sinks). Similarly, to the previous experiment, the same temperature curves were obtained; however, the voltage output of the TEG was measured in the range of 0.3 V and 1.1 V, which is smaller than the theoretically estimated voltage output. The TEG voltage and temperature parameters are shown in Figure 24.

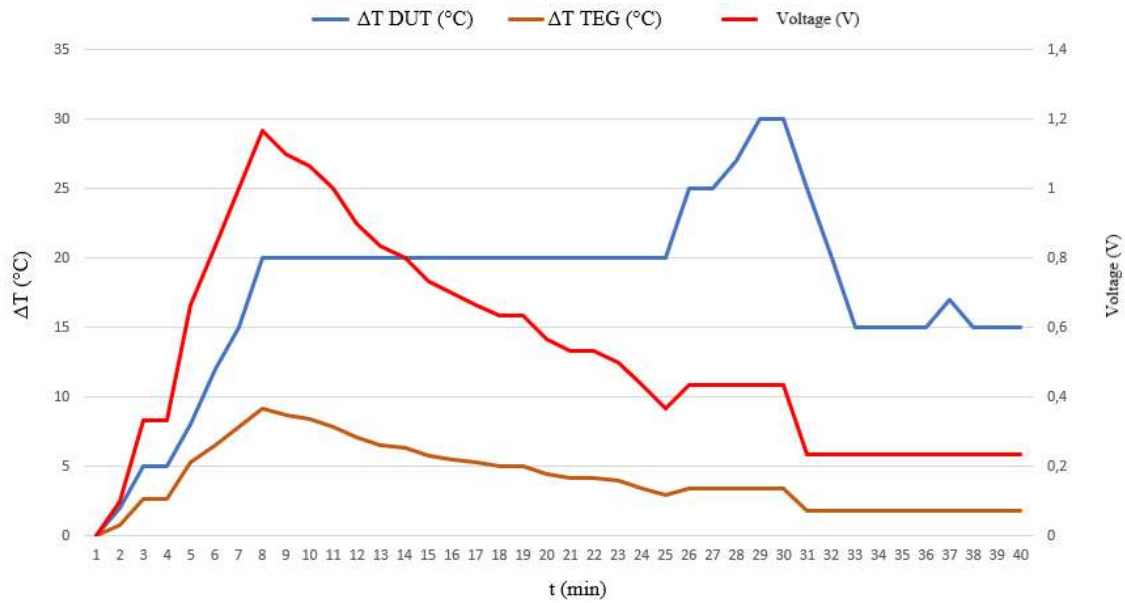


Figure 24: Measurement results with the Peltier elements organized as 3 rows wherein the 5 elements connected in series and the rows are connected in parallel, for the purpose of increasing the current output I_{TEG_max} (schematic of Figure 23): measured voltage output Voltage (V) of the TEG (red line), temperature difference of the DUT surface and ambient temperature ΔT (°C) (blue line) and temperature difference between hot and cold side of the TEG ΔT (°C) (brown line).

The current output result obtained is $I_{OUT_max} = 0.34 A$ at the maximum temperature difference and $I_{OUT_max} = 0.09 A$. Therefore, the power output of the TEG in this assembly is in the range of $0.102 W$ and $0.374 W$.

Finally, the output from the single Peltier element of the TEG has been measured. It was observed that the maximum voltage level was $0.25 V$, decreased quickly to $0.05 V$ and remains stable at this level. Figure 25 shows the temperature and voltage output parameters of a single Peltier element of the TEG.

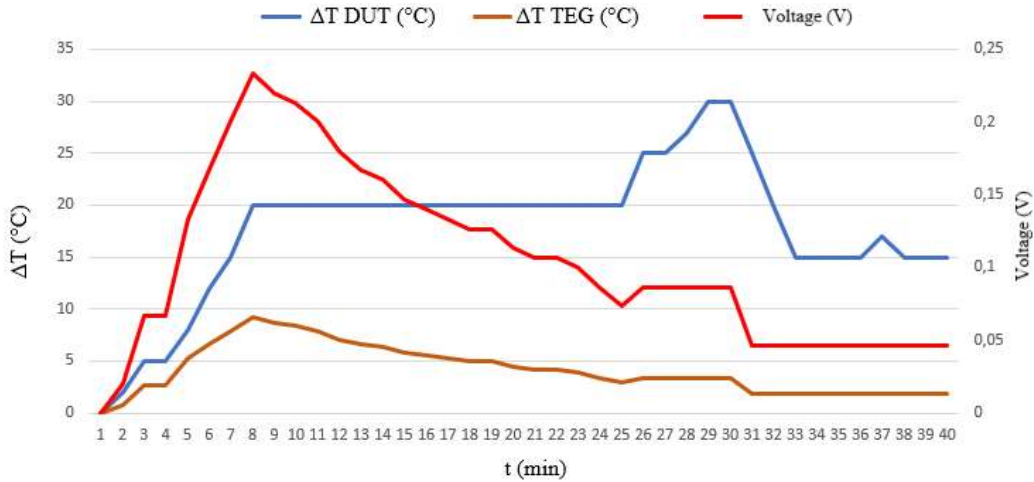


Figure 25: Measurement results on one single Peltier element on the TEG (one element from the schematic of Figure 23): measured voltage output Voltage (V), (red line), temperature difference of the DUT surface and ambient temperature ΔT (°C) (blue line) and temperature difference between hot and cold side of the TEG ΔT (°C) (brown line).

For the maximum output current obtained is $0.1 A$ at the maximum and $0.02 A$ at the minimum, so the power of the single TEG element estimated at the range of $0.001 W$ and $0.022 W$.

During experiments it was observed that with the proposed and developed TEG assembly, it is practically difficult to achieve the theoretically estimated results due to TEG surfaces mutual heat effect. However, it was observed that ΔT of the hot and cold sides of TEG reaches its minimum of $2\text{ }^{\circ}\text{C}$ in both experiments and does not fall further. Additionally, it was verified that during the extension of the experiments time to 60 min, the temperature difference on the cold and hot sides of the TEG remains stable, and the voltage outputs remain stable too, i.e. in case of series connection, the output level stabilises at $0.7 V$ and in case of parallel connection, it stabilises at $0.3 V$; finally, for a single Peltier element the output level is stabilised at $0.05 V$, all during 30 min of each experiment.

5.2 Experiments on TEG effectiveness

To measure the real effectiveness of the TEG, first it is required to estimate the figure of merit (ZT , see Section 4.2.2). To do that, it is required to measure the Seebeck coefficient by measuring the real temperature difference and the output voltage, and then by deriving Seebeck coefficient from Equation (1) $\alpha_{AB} = \frac{V_{out}}{N \cdot \Delta T}$. So, the measured Seebeck coefficient for both TEG assemblies (with elements connected in series and elements connected in parallel) is $\alpha_{AB} = 0.0002 \text{ V}/^\circ\text{K}$ or $200 \times 10^{-6} \text{ V}/^\circ\text{K}$, which corresponds the theoretical value. Then it is required to measure the total electrical resistivity of the TEG. The single TEC resistivity measured is $R_g = 1.91 \text{ } \Omega$, so it is less than the TEC (Peltier element) datasheet value ($R_g = 2.05 \text{ } \Omega$) [49]. The total resistivity of the TEG in case of series connection is $R_{TEG_total} = 28.65 \text{ } \Omega$ and $R_{TEG_total} = 3.18 \text{ } \Omega$ in case of parallel arrays connection. Taking those values, it is possible to evaluate the FOM, which is $ZT = 1.57$. Therefore, with temperature ranges from experiments, the effectiveness of the TEG can be calculated with Equation (7); the result is shown in Figure 26.

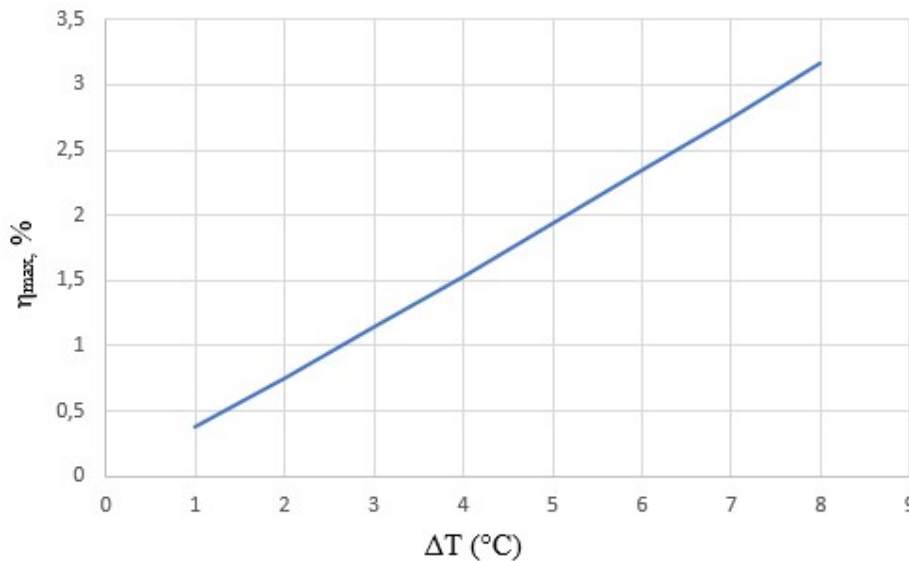


Figure 26: TEG effectiveness calculation based on the experimental results; η_{max} % is the effectiveness of the TEG and ΔT (°C) is the temperature difference obtained on the TEG cold and hot surfaces.

As can be seen from the plot based on measurements, the maximum effectiveness of the TEG obtained in the experiments is between 0.5 % and 3.2 %, which could be explained as a result of the low temperature difference (ΔT) between hot and cold side of the TEG.

The area of the TEG assembly is 412 cm^2 and the power level for TEG elements in series connection is in the range of $0.014 - 0.42 \text{ W}$, so the power density of the TEG is in the range of $30 \mu\text{W}/\text{cm}^2$ and $10 \text{ mW}/\text{cm}^2$. For the parallel assembly, the power density is in the range of $2 \text{ mW}/\text{cm}^2$ and $9 \text{ mW}/\text{cm}^2$. Therefore, the measured power density of the designed TEG is corresponding the theoretically estimated levels, listed in Table 1 in Chapter 2.

Practical experiments with the TEG have confirmed its concept of effectiveness estimation and main working principles, including dependencies on ΔT and power output parameters. However, the real-life experiments show that it is difficult to keep ΔT on the same level during an extended amount of time as long as the output power parameters. Along with that, it was also observed that even a relatively low temperature difference remains at the hot and cold sides of the TEG for 30 min and even more, which allows to keep voltage output stable.

5.3 Experiments with the TEG output conversion

Since the TEG output is not stable, additional experiments with the DC converter were conducted to verify the DC converter functionality and verify the SPICE simulation results described in Chapter 4.

The goal of the experiment is to check the functionality of the DC converter in practice, compare the practical results with simulations results and measure the total maximum output of the DC converter, as well is to verify how stable is the output.

The assembled circuit is connected to the TEG output and the experiments from Section 5.2 were repeated with the DC converter.

The first experiment conducted with TEG where all Peltier elements are connected in series. From the previous experiments with the TEG, it was observed that the voltage output of the TEG is 3.5 V , and the minimum voltage output is 0.7 V . The maximum output voltage at this level falls into the maximum power rating of LTC3108, so it is not recommended to supply the DC converter during the long time.

The measurements at the output of the DC converter were done with the multimeter at outputs V_{out} and V_{LDO} . From the experiment it is observable that the V_{out} of the DC

converter reaches its maximum of 5 V at the beginning of the experiment and V_{LDO} reaches its maximum of 2.2 V and remains stable during the experiment until the test is finished. The results are plotted on the chart shown in Figure 27.



Figure 27: DC converter output graph for TEG elements connected in series. The TEG output is represented with the red line and labelled as V_{teg_out} , DC converter V_{out} is represented with the blue line (labelled as V_{out}) and V_{LDO} output of DC converter is represented with the brown line (labelled V_{ldo}).

The experiment results correspond the SPICE simulation results, and the DC converter output V_{out} (blue line on the chart) remains stable at the level of 5 V; since the DC converter input remains stable during the experiment and does not drop lower than 0.7 V (red line on the chart), the DC converter is able to operate at its maximum level without voltage decrease at the outputs. V_{LDO} (brown line on the chart, labelled “ V_{ldo} ”) output remains stable at 2.2 V as expected.

The next experiment is aimed at verifying the DC converter functionality with the TEG, where the elements are connected in series and parallel configuration (as was shown in Figure 23). After the TEG cooled down, its output is connected to the DC converter input, and the test executed again. The result of the experiment is plotted on the chart shown in Figure 28.

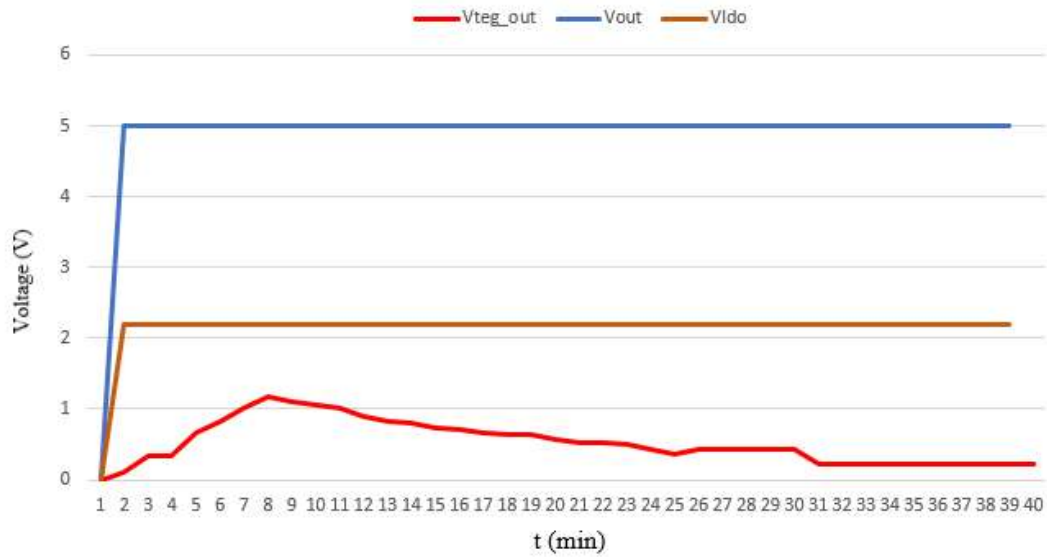


Figure 28: DC converter output graph for TEG elements, connected in series and parallel. The TEG output is represented with the red line and labelled as Vteg_out, the DC converter V_{out} is represented with the blue line (labelled as Vout) and the V_{LDO} output of DC converter is represented with the brown line (labelled Vldo).

As the TEG voltage output remains stable at 0.3 V (red line on the chart, labelled as “Vteg_out”), the DC converter operates at its maximum and V_{out} (blue line on the chart, labelled as “Vout”) remains stable at the level of 5 V. V_{LDO} (brown line on the chart, labelled “Vldo”) output remains stable at 2.2 V as expected. The obtained results correspond to the SPICE simulation results.

The next experiment is aimed at measuring the DC converter output when a single Peltier of the TEG is connected to DC converter input. This is required to verify if a single TEC could drive the DC converter at its maximum. To do that, the TEG was cooled down, and the test executed again. During the experiment, the TEC output was measured, as well as V_{LDO} and V_{out} outputs of the DC converter. The result is plotted on the graph shown in Figure 29.

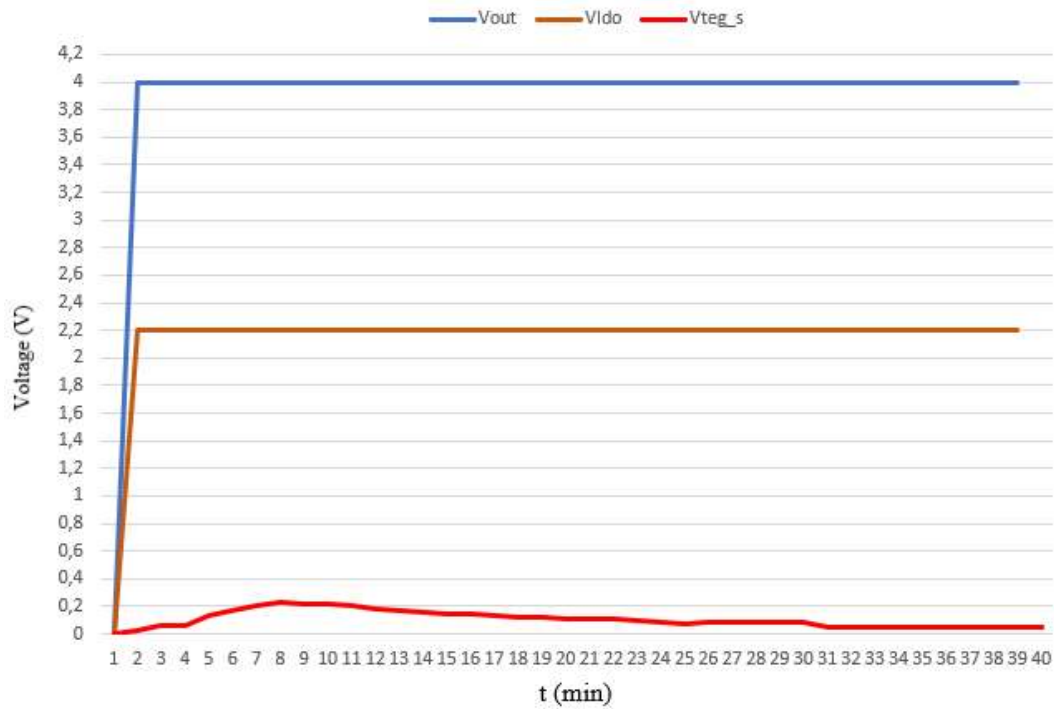


Figure 29: DC converter output graph for a single Peltier element of TEG. TEG Peltier element output is represented with red line and labelled as V_{teg_s} , DC converter V_{out} represented as blue line (labelled as V_{out}) and VLDO output of DC converter represented with brown line (labelled V_{ldo}).

The obtained results show that the output from the single Peltier element is in the range of $0.04 - 0.2\text{ V}$ (red line on the chart, labelled “ V_{teg_s} ”), which is larger than minimum start-up DC converter voltage (0.02 V); however, the maximum output of the DC converter could not be reached: V_{out} remains at the level of 4 V (blue line on the chart, labelled “ V_{out} ”), and V_{LDO} remains stable at the level of 2.2 V (brown line on the chart, labelled “ V_{ldo} ”).

The set of experiments with the LTC3108 DC converter were conducted and the results show that the DC converter works as specified, i.e., the outputs are stable, and the obtained practical experiments results correspond to the SPICE simulation results.

5.4 Discussion of the results

The main goal of the experiments was to verify the main parameters of the TEG and the TEG output conversion results. Another goal was to check, in practice, the previously theoretically estimated parameters, such as TEG effectiveness, working parameters under different temperatures and their influence on the TEG output. All experiments were done under certain temperature levels since the heat source (radio equipment DUT) available has limited temperature ranges. Moreover, all the experiments were done during a restricted amount of time (40 min), which corresponds to the time of the DUT test procedure selected for the experiments. It was assumed that these limited conditions will allow to harvest only limited amount of power, so the measurements done in the experiments were aimed to measure and estimate these limits.

The experiments have proven that the main disadvantage of the TEG assembly and of the TEC element itself is the mutual temperature flow between the hot and cold sides, which leads to the TEG power output decrease rapidly in a short amount of time. At low temperature levels and temperature differences, the obtained TEG effectiveness maximum was 3.2 %. The measured power densities of the TEG were $30 \mu W/cm^2$ to $10 mW/cm^2$ which correspond to the theoretical values.

The results of the experiments with the proposed LTC3108 based DC converter shown that it is possible to obtain a stable voltage output during a considerable amount of time (40 min) at the level of 5 V without fluctuations. However, considering the TEG output levels, this brings a restriction to use such a DC converter at high TEG output levels (3.5 V at maximum), which makes this DC converter not versatile for any TEG assembly.

Therefore, since the DC rectifier cannot handle the voltage from the assembly connected in series, a single TEG cannot not provide proper voltage level to drive the DC converter to provide maximum output; based on the analysis of the obtained results, it is expected that the optimal energy conversion schematics for the proposed TEG is to use each 5 Peltier elements, connected in series, and connected to DC rectifier, so in total for proposed TEG it would be required to connect 3 DC rectifiers. The schematic representation of this connection configuration is shown on Figure 30.

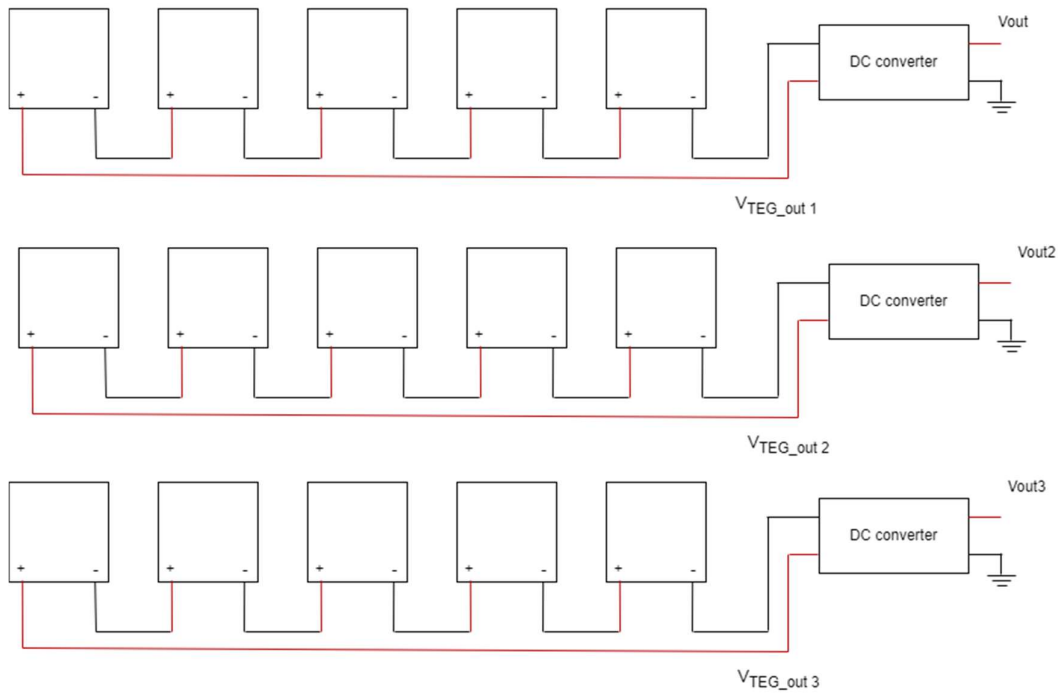


Figure 30: Proposed energy conversion schematic with 3 DC converters, connected to 5 Peltier elements each. The Peltier elements are connected in series. $V_{TEG_out\ 1}$ is the output from the first 5 Peltier elements in the top row, $V_{TEG_out\ 2}$ is the output from the second 5 Peltier elements in the middle row, and $V_{TEG_out\ 3}$ is the output from the third 5 Peltier elements in the bottom row. V_{out} , V_{out2} and V_{out3} are the outputs from the first, second, and third DC converter, respectively.

A TEH solution assembled with this schematic would be expected to allow increasing total level of voltage output, and at the same time is capable to drive the DC converter at its maximum power rating during the long amount of time with a stable output.

This chapter described the practical experiments with thermal EH solution, consisting of TEG and DC converter, including the output and effectiveness parameters measurements, main thermal parameters, and influence of thermal parameters of the heat source to the electrical output. All in all, with the conducted experiments, the proposed thermal EH solution has been assessed and the outcomes of the experiments correspond to the parameters calculated theoretical values and simulated values.

The next chapter concludes this MSc thesis with a summary and suggestions for further work.

6 Conclusion

In this MSc thesis, potential energy harvesting methods have been investigated to be used in a telecom company during the radio equipment testing process, as a part of the development of their energy efficiency strategies. This work has focused on exploring and analysing the suitable EH methods which could be applicable in the telecom company. Though the scope of this thesis has mostly focused on thermal energy harvesting method testing operations, RF energy sources were also initially investigated; however, during the field work it was found out that RF EH solutions could not be implemented as they bring incompatibilities into the existing internal telecom company process and could significantly impair the precise measurements that must be taken during testing operations. Therefore, thermal energy harvesting has been further investigated as the only available and applicable method for energy harvesting in this telecom company.

6.1 Summary and main findings

In summary, during this work it was studied and investigated the common EH approaches and methods, of which thermal energy harvesting was studied in more details. Although research in this domain receives significant interest nowadays and many papers are available on the topic, TEH still raises misconceptions because many factors influence the overall idea and practical feasibility. In general TEH is used for low-power IoT solutions; contrary to this, the main goal of this thesis was to investigate whether this method to be used in a telecom company. To do so, it was crucial to overview main concepts of the TEH, investigate common approaches and assess them with simulations and experiment.

The experiments conducted in this MSc thesis have shown that the TEH method could provide a meaningful amount of harvested energy, so this method could be recommended to use. Conventional TEH approaches are focused mostly on increasing the temperature difference on TEGs to achieve better output characteristics, although in this work it was identified that even with low temperature levels it is possible to harvest relevant amount of energy with by increased TEG area.

The experiments with DC converters have shown that energy conversion is the one of the most important parts of the EH solution and it also significantly influences the TEH effectiveness.

Based on the achieved results, it is concluded that the initial goal of this MSc thesis has been reached. Some recommendations for furthering this work are presented in what follows.

6.2 Recommendations for further work

It should be noted that further research is needed to fully explore the potential of energy harvesting in general and thermal energy harvesting in particular to overcome some of the challenges associated with this technology, such as the need for more efficient materials, power conversion and management, and energy storage.

It is recommended to continue research and development work to explore the availability of thermal sources to be used for energy harvesting. It is also recommended to improve the proposed TEG EH solution by creating scalable devices and power output management, based on the principles described in this work, taking into consideration the findings and experiments results.

Additionally, as this MSc thesis outlined the challenges on energy conversion, it is recommended to continue studies on possible alternative circuits to improve the characteristics of DC conversion modules.

Energy storage and reuse of stored energy is the subject of separate research since this matter brings a key value to the overall EH concept. Several approaches are possible to achieve this, such as finding the way to store the harvested energy to small scale local grids, batteries, or even supercapacitors.

References

- [1] European Commission, “Communication and roadmap on the European Green Deal.” Brussels, Jan. 15, 2020.
- [2] “United Nations Framework Convention on Climate Change. (2016). Paris Agreement.,” <https://unfccc.int/process-and-meetings/the-paris-agreement/the-paris-agreement>, Dec. 12, 2016.
- [3] “Directive (EU) 2018/2001 of the European Parliament and of the Council of 11 December 2018 on the promotion of the use of energy from renewable sources, OJ L 328, 21.12.2018.”
- [4] “Directive 2012/27/EU of the European Parliament and of the Council of 25 October 2012 on energy efficiency, OJ L 315, 14.11.2012.”
- [5] L.-G. Tran, H.-K. Cha, and W.-T. Park, “RF power harvesting: a review on designing methodologies and applications,” *Micro and Nano Systems Letters*, vol. 5, no. 1, p. 14, Dec. 2017, doi: 10.1186/s40486-017-0051-0.
- [6] M. Prauzek, J. Konecny, M. Borova, K. Janosova, J. Hlavica, and P. Musilek, “Energy Harvesting Sources, Storage Devices and System Topologies for Environmental Wireless Sensor Networks: A Review,” *Sensors*, vol. 18, no. 8, p. 2446, Jul. 2018, doi: 10.3390/s18082446.
- [7] A. O. Ochieng, T. F. Megahed, S. Ookawara, and H. Hassan, “Comprehensive review in waste heat recovery in different thermal energy-consuming processes using thermoelectric generators for electrical power generation,” *Process Safety and Environmental Protection*, vol. 162, pp. 134–154, Jun. 2022, doi: 10.1016/j.psep.2022.03.070.
- [8] M. Deymi-Dashtebayaz and S. Valipour-Namanlo, “Thermoeconomic and environmental feasibility of waste heat recovery of a data center using air source heat pump,” *J Clean Prod*, vol. 219, pp. 117–126, May 2019, doi: 10.1016/j.jclepro.2019.02.061.
- [9] S. Zeadally, F. K. Shaikh, A. Talpur, and Q. Z. Sheng, “Design architectures for energy harvesting in the Internet of Things,” *Renewable and Sustainable Energy Reviews*, vol. 128, p. 109901, Aug. 2020, doi: 10.1016/J.RSER.2020.109901.
- [10] E. Brownell and M. Hodes, “Optimal Design of Thermoelectric Generators Embedded in a Thermal Resistance Network,” *IEEE Trans Compon Packaging Manuf Technol*, vol. 4, no. 4, pp. 612–621, Apr. 2014, doi: 10.1109/TCPMT.2013.2295169.
- [11] C. Goupil, W. Seifert, K. Zabrocki, E. Müller, and G. J. Snyder, “Thermodynamics of Thermoelectric Phenomena and Applications,” *Entropy*, vol. 13, no. 8, pp. 1481–1517, Aug. 2011, doi: 10.3390/e13081481.

- [12] K. T. Settaluri, H. Lo, and R. J. Ram, “Thin Thermoelectric Generator System for Body Energy Harvesting,” *J Electron Mater*, vol. 41, no. 6, pp. 984–988, Jun. 2012, doi: 10.1007/s11664-011-1834-3.
- [13] N. Jaziri, A. Boughamoura, J. Müller, B. Mezghani, F. Tounsi, and M. Ismail, “A comprehensive review of Thermoelectric Generators: Technologies and common applications,” *Energy Reports*, vol. 6, pp. 264–287, Dec. 2020, doi: 10.1016/j.egy.2019.12.011.
- [14] P. Nintanavongsa, “A Survey on RF Energy Harvesting: Circuits and Protocols,” *Energy Procedia*, vol. 56, no. C, pp. 414–422, Jan. 2014, doi: 10.1016/J.EGYPRO.2014.07.174.
- [15] X. Lu, P. Wang, D. Niyato, D. I. Kim, and Z. Han, “Wireless Networks With RF Energy Harvesting: A Contemporary Survey,” *IEEE Communications Surveys & Tutorials*, vol. 17, no. 2, pp. 757–789, 2015, doi: 10.1109/COMST.2014.2368999.
- [16] T. Soyata, L. Copeland, and W. Heinzelman, “RF Energy Harvesting for Embedded Systems: A Survey of Tradeoffs and Methodology,” *IEEE Circuits and Systems Magazine*, vol. 16, no. 1, pp. 22–57, 2016, doi: 10.1109/MCAS.2015.2510198.
- [17] H. H. Ibrahim *et al.*, “Radio Frequency Energy Harvesting Technologies: A Comprehensive Review on Designing, Methodologies, and Potential Applications,” *Sensors*, vol. 22, no. 11, p. 4144, May 2022, doi: 10.3390/s22114144.
- [18] B. Maamer, A. Boughamoura, A. M. R. Fath El-Bab, L. A. Francis, and F. Tounsi, “A review on design improvements and techniques for mechanical energy harvesting using piezoelectric and electromagnetic schemes,” *Energy Convers Manag*, vol. 199, p. 111973, Nov. 2019, doi: 10.1016/J.ENCONMAN.2019.111973.
- [19] N. Sezer and M. Koç, “A comprehensive review on the state-of-the-art of piezoelectric energy harvesting,” *Nano Energy*, vol. 80, p. 105567, Feb. 2021, doi: 10.1016/J.NANOEN.2020.105567.
- [20] A. Muscat, S. Bhattacharya, and Y. Zhu, “Electromagnetic Vibrational Energy Harvesters: A Review,” *Sensors*, vol. 22, no. 15, p. 5555, Jul. 2022, doi: 10.3390/s22155555.
- [21] R. Lensvelt, R. H. B. Fey, R. M. C. Mestrom, and H. Nijmeijer, “Design and Numerical Analysis of an Electrostatic Energy Harvester With Impact for Frequency Up-Conversion,” *J Comput Nonlinear Dyn*, vol. 15, no. 5, May 2020, doi: 10.1115/1.4046664.
- [22] B. Kumar, “Global Energy Harvesting System Market – Analysis and Forecast (2018 – 2024),” Jan. 2019.

- [23] E. P. Nikhil M, “Energy Harvesting System Market by Technology (Light Energy Harvesting, Vibration Energy Harvesting, Radio Frequency Energy Harvesting, and Thermal Energy Harvesting), Component (Energy Harvesting Transducers, Power Management Integrated Circuits (PMIC), and Storage System), and Application (Building & Home Automation, Consumer Electronics, Industrial, Transportation, and Others): Global Opportunity Analysis and Industry Forecast, 2021-2030,” 2021.
- [24] A. Cuneo, S. Barberis, A. Traverso, and P. Silvestri, “Market opportunities for small energy harvesters,” *E3S Web of Conferences*, vol. 113, p. 03010, Aug. 2019, doi: 10.1051/e3sconf/201911303010.
- [25] “TEG12VDC-AIR (FORCED AIR COOLING).” [Online]. Available: www.tecteg.com
- [26] I. Ahmad, L. M. Hee, A. M. Abdelrhman, S. A. Imam, and M. S. Leong, “Scopes, challenges and approaches of energy harvesting for wireless sensor nodes in machine condition monitoring systems: A review,” *Measurement*, vol. 183, p. 109856, Oct. 2021, doi: 10.1016/j.measurement.2021.109856.
- [27] R. De Fazio, M. De Giorgi, D. Cafagna, C. Del-Valle-Soto, and P. Visconti, “Energy Harvesting Technologies and Devices from Vehicular Transit and Natural Sources on Roads for a Sustainable Transport: State-of-the-Art Analysis and Commercial Solutions,” *Energies (Basel)*, vol. 16, no. 7, p. 3016, Mar. 2023, doi: 10.3390/en16073016.
- [28] P. Visconti, N. I. Giannoccaro, and R. de Fazio, “Special Issue on Electronic Systems and Energy Harvesting Methods for Automation, Mechatronics and Automotive,” *Energies (Basel)*, vol. 14, no. 23, p. 8050, Dec. 2021, doi: 10.3390/en14238050.
- [29] M. Jia, E. H. M. Sha, Q. Zhuge, and S. Gu, “Transient computing for energy harvesting systems: A survey,” *Journal of Systems Architecture*, vol. 132, p. 102743, Nov. 2022, doi: 10.1016/J.SYSARC.2022.102743.
- [30] T.-C. Cheng, C.-H. Cheng, Z.-Z. Huang, and G.-C. Liao, “Development of an energy-saving module via combination of solar cells and thermoelectric coolers for green building applications,” *Energy*, vol. 36, no. 1, pp. 133–140, Jan. 2011, doi: 10.1016/j.energy.2010.10.061.
- [31] R. J. M. Vullers, R. van Schaijk, I. Doms, C. Van Hoof, and R. Mertens, “Micropower energy harvesting,” *Solid State Electron*, vol. 53, no. 7, pp. 684–693, Jul. 2009, doi: 10.1016/j.sse.2008.12.011.
- [32] S. B. Riffat and X. Ma, “Thermoelectrics: a review of present and potential applications,” *Appl Therm Eng*, vol. 23, no. 8, pp. 913–935, Jun. 2003, doi: 10.1016/S1359-4311(03)00012-7.

- [33] M. E. Kiziroglou and E. M. Yeatman, "Materials and techniques for energy harvesting," in *Functional Materials for Sustainable Energy Applications*, Elsevier, 2012, pp. 541–572. doi: 10.1533/9780857096371.4.539.
- [34] D. Champier, "Thermoelectric generators: A review of applications," *Energy Convers Manag*, vol. 140, pp. 167–181, May 2017, doi: 10.1016/j.enconman.2017.02.070.
- [35] H. Kaibe, K. Makino, T. Kajihara, S. Fujimoto, and H. Hachiuma, "Thermoelectric generating system attached to a carburizing furnace at Komatsu Ltd., Awazu Plant," 2012, pp. 524–527. doi: 10.1063/1.4731609.
- [36] O. H. Ando Junior, A. L. O. Maran, and N. C. Henao, "A review of the development and applications of thermoelectric microgenerators for energy harvesting," *Renewable and Sustainable Energy Reviews*, vol. 91, pp. 376–393, Aug. 2018, doi: 10.1016/j.rser.2018.03.052.
- [37] W. Wang, V. Cionca, N. Wang, M. Hayes, B. O'Flynn, and C. O'Mathuna, "Thermoelectric Energy Harvesting for Building Energy Management Wireless Sensor Networks," *Int J Distrib Sens Netw*, vol. 9, no. 6, p. 232438, Jun. 2013, doi: 10.1155/2013/232438.
- [38] S. Kim *et al.*, "Ambient RF Energy-Harvesting Technologies for Self-Sustainable Standalone Wireless Sensor Platforms," *Proceedings of the IEEE*, vol. 102, no. 11, pp. 1649–1666, Nov. 2014, doi: 10.1109/JPROC.2014.2357031.
- [39] V. Marian, B. Allard, C. Vollaie, and J. Verdier, "Strategy for Microwave Energy Harvesting From Ambient Field or a Feeding Source," *IEEE Trans Power Electron*, vol. 27, no. 11, pp. 4481–4491, Nov. 2012, doi: 10.1109/TPEL.2012.2185249.
- [40] R. J. Vyas, B. B. Cook, Y. Kawahara, and M. M. Tentzeris, "E-WEHP: A Batteryless Embedded Sensor-Platform Wirelessly Powered From Ambient Digital-TV Signals," *IEEE Trans Microw Theory Tech*, vol. 61, no. 6, pp. 2491–2505, Jun. 2013, doi: 10.1109/TMTT.2013.2258168.
- [41] R. K. Sidhu, J. Singh Ubhi, and A. Aggarwal, "A Survey Study of Different RF Energy Sources for RF Energy Harvesting," in *2019 International Conference on Automation, Computational and Technology Management (ICACTM)*, IEEE, Apr. 2019, pp. 530–533. doi: 10.1109/ICACTM.2019.8776726.
- [42] M. Pinuela, P. D. Mitcheson, and S. Lucyszyn, "Ambient RF Energy Harvesting in Urban and Semi-Urban Environments," *IEEE Trans Microw Theory Tech*, vol. 61, no. 7, pp. 2715–2726, Jul. 2013, doi: 10.1109/TMTT.2013.2262687.
- [43] P. T. Thakar, N. Shah, R. Shah, V. Sharma, and Y. Bandi, "Antenna-Based RF Energy Harvesting," 2020, pp. 481–491. doi: 10.1007/978-981-15-1002-1_49.

- [44] M. Basim *et al.*, “A Highly Efficient RF-DC Converter for Energy Harvesting Applications Using a Threshold Voltage Cancellation Scheme,” *Sensors*, vol. 22, no. 7, p. 2659, Mar. 2022, doi: 10.3390/s22072659.
- [45] H. Q. Nguyen and M. T. Le, “Multiband Ambient RF Energy Harvester with High Gain Wideband Circularly Polarized Antenna toward Self-Powered Wireless Sensors,” *Sensors*, vol. 21, no. 21, p. 7411, Nov. 2021, doi: 10.3390/s21217411.
- [46] P. D. Mitcheson, S. Lucyszyn, M. P. Rangel, and D. C. Yates, “Patent, RF ENERGY HARVESTER,” US 2016/0181873 A1, 2016
- [47] N. Shariati, W. S. T. Rowe, and K. Ghorbani, “Highly sensitive rectifier for efficient RF energy harvesting,” in *2014 44th European Microwave Conference*, IEEE, Oct. 2014, pp. 1190–1193. doi: 10.1109/EuMC.2014.6986654.
- [48] M. M. Mnif, H. Mnif, and M. Loulou, “New design of RF-DC rectifier circuit for radio frequency energy harvesting,” in *2016 IEEE International Conference on Electronics, Circuits and Systems (ICECS)*, IEEE, Dec. 2016, pp. 664–667. doi: 10.1109/ICECS.2016.7841289.
- [49] T. M. Tritt and M. A. Subramanian, “Thermoelectric Materials, Phenomena, and Applications: A Bird’s Eye View,” *MRS Bull*, vol. 31, no. 3, pp. 188–198, Mar. 2006, doi: 10.1557/mrs2006.44.
- [50] Mouser Electronics, “ATS-TEC40-39-004 Datasheet,” *Datasheet*, 2014.
- [51] S. Bhattacharya, H. Behlow, I. Rancu, A. M. Rao, and H. J. Goldsmid, “Thermoelectric figure-of-merit from Peltier cooling,” *J Appl Phys*, vol. 132, no. 17, p. 175106, Nov. 2022, doi: 10.1063/5.0116327.
- [52] K. Kakollu Manoj Kumar, “Combined Efficiency Calculation of Bismuth Telluride and Lead Telluride in Thermoelectric Module,” *Journal Of Modern Engineering Research (IJMER)* , vol. 7, no. 1, pp. 46–52, 2017.
- [53] H. Goldsmid, “Bismuth Telluride and Its Alloys as Materials for Thermoelectric Generation,” *Materials*, vol. 7, no. 4, pp. 2577–2592, Mar. 2014, doi: 10.3390/ma7042577.
- [54] A. Nozariasbmarz, B. Poudel, W. Li, H. B. Kang, H. Zhu, and S. Priya, “Bismuth Telluride Thermoelectrics with 8% Module Efficiency for Waste Heat Recovery Application,” *iScience*, vol. 23, no. 7, p. 101340, Jul. 2020, doi: 10.1016/j.isci.2020.101340.
- [55] S. A. Afghan and H. Géza, “Modelling and Analysis of Energy Harvesting in Internet of Things (IoT): Characterization of a Thermal Energy Harvesting Circuit for IoT based Applications with LTC3108,” *Energies (Basel)*, vol. 12, no. 20, p. 3873, Oct. 2019, doi: 10.3390/en12203873.

- [56] Linear Technologies, “LTC3108 Ultralow Voltage Step-Up Converter and Power Manager.” [Online]. Available: <https://www.analog.com/media/en/technical-documentation/data-sheets/3108fc.pdf>

Appendix 1 – Non-exclusive licence for reproduction and publication of a graduation thesis¹

I Aleksei Veselkov

1. Grant Tallinn University of Technology free licence (non-exclusive licence) for my thesis” Investigation of Energy Harvesting Methods During Testing Operations at a Telecom Company”, supervised by Yannick Le Moullec and Salvador Gonzalez Perez
 - 1.1. to be reproduced for the purposes of preservation and electronic publication of the graduation thesis, incl. to be entered in the digital collection of the library of Tallinn University of Technology until expiry of the term of copyright;
 - 1.2. to be published via the web of Tallinn University of Technology, incl. to be entered in the digital collection of the library of Tallinn University of Technology until expiry of the term of copyright.
2. I am aware that the author also retains the rights specified in clause 1 of the non-exclusive licence.
3. I confirm that granting the non-exclusive licence does not infringe other persons' intellectual property rights, the rights arising from the Personal Data Protection Act or rights arising from other legislation.

06.05.2023

¹ The non-exclusive licence is not valid during the validity of access restriction indicated in the student's application for restriction on access to the graduation thesis that has been signed by the school's dean, except in case of the university's right to reproduce the thesis for preservation purposes only. If a graduation thesis is based on the joint creative activity of two or more persons and the co-author(s) has/have not granted, by the set deadline, the student defending his/her graduation thesis consent to reproduce and publish the graduation thesis in compliance with clauses 1.1 and 1.2 of the non-exclusive licence, the non-exclusive license shall not be valid for the period.